NASA TN D-1459

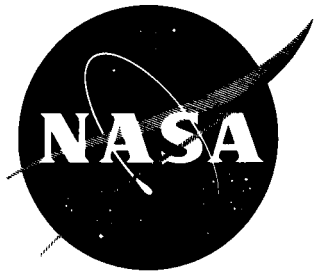

TECHNICAL NOTE

D-1459

EFFECTS OF AIR CONTENT AND WATER PURITY ON LIQUID TENSION AT INCIPIENT CAVITATION IN VENTURI FLOW

By Robert S. Ruggeri and Thomas F. Gelder

Lewis Research Center
Cleveland, Ohio

NATIONAL AERONAUTICS AND SPACE ADMINISTRATION
WASHINGTON
March 1963

NATIONAL AERONAUTICS AND SPACE ADMINISTRATION

TECHNICAL NOTE D-1459

EFFECTS OF AIR CONTENT AND WATER PURITY ON LIQUID TENSION AT INCIPIENT CAVITATION IN VENTURI FLOW

By Robert S. Ruggeri and Thomas F. Gelder

SUMMARY

Cavitation of demineralized, tap, and distilled water was induced on the walls of a venturi having a 1.377-inch throat diameter in a closed-return liquid tunnel. The occurrence and magnitude of local tensile stresses in the liquid at incipient-cavitation conditions were studied over a range of air content. Local tensile stresses at incipience of visible cavitation were independent of water type and air content and ranged from 5 to 23 feet of water for free-stream velocities from 20 to 45 feet per second, respectively. Tensile stresses at incipience of audible cavitation varied considerably with air content of the water but were generally less than those obtained at the visible threshold. Visible incipient cavitation was of the fixed type and always occurred as a practically instantaneous burst of vapor bubbles in the region of minimum pressure. Venturi cavitation was unsteady for all degrees of cavitation and stream velocities studied.

INTRODUCTION

Cavitation, or the formation and collapse of cavities in a flowing liquid caused by pressure changes (due to velocity changes), often results in mechanical damage, noise, and degrading of the flow pattern with consequent reduction in component performance. It is generally assumed that cavitation will occur when local pressures equal the vapor pressure of the liquid; hence, to avoid the undesirable effects of cavitation, flow boundaries are usually designed to maintain minimum pressures at levels above vapor pressure. If cavitation can be delayed to pressures less than vapor pressure, higher relative flow velocities may be employed, and size and weight reductions in plumbing or efficiency gains in rotating machinery may be realized.

If a liquid will flow through a region wherein local pressures are less than vapor pressure without apparent cavitation, the liquid is considered to have sustained, for all engineering purposes, a tensile stress. The magnitude of this effective tensile stress is taken to be the difference between the minimum local pressure and vapor pressure. Water, for example, is capable of supporting considerable tensile stress; as stated in reference 1, (1) almost any water will sustain a tensile stress for a short time, and (2) completely pure, gas-free water kept very still will sustain tension indefinitely. Tensile stresses from

3 to 60 feet of water head near or at cavitation inception are reported in references 2 to 5 for flowing systems using various models and unmodified fresh water over a range of air contents.

The purpose of the present investigation is to study in a flowing system the occurrence and magnitude of tensile stresses near or at cavitation inception, as affected by demineralized, tap, and distilled fresh waters, each over a range of air contents. The study was conducted at the NASA Lewis Research Center as part of a general program in cavitation research. Cavitation was induced on the walls of a transparent venturi test section (throat diam., 1.377 in.) in a closed-return liquid tunnel. The venturi, designed to minimize the time the flowing water is exposed to low local pressures, incorporates a wall profile on which the minimum pressure is well below that elsewhere in the tunnel circuit. Further, this minimum pressure region extends for only a short distance in the flow direction. With this venturi, local pressures were obtained for evaluation of local tensile stresses in water at incipient-cavitation conditions. Cavitation inception was determined both visually and audibly. (Visible and audible incipient cavitation do not necessarily occur simultaneously.) The three waters were studied over the following range of variables: free-stream velocity from 19 to 45 feet per second; free-stream static pressure head from 15 to 98 feet of water absolute; temperature from 67° to 110° F; and absolute air content (by weight) from about 1.4 to 26.3 milligrams of air per kilogram of water.

APPARATUS

The facility used in the present study is a small closed-return liquid tunnel; a photograph and schematic drawing are shown in figures 1(a) and (b), respectively. The upper leg of the tunnel contains 12-inch-long working sections having maximum internal diameters of 1.743 inches. All tunnel components, where practical, were machined from aluminum rod (6061-T6) to minimize welding. A hard anodic coating was applied to all aluminum tunnel and pump parts to avoid corrosion. Bore alinements were held to ±0.001 inch by flange pilots, and neoprene- or Teflon-coated aluminum O-rings were used as seals. Three sets of corner-turning vanes, three "eggcrate" flow straighteners, and two sets of stainless-steel screens were used, all to favor the attainment of uniform, steady, irrotational flow at the working section (see fig. 1(b)). To minimize the possibility of flow separation within the tunnel circuit, all diffuser sections have a half-angle divergence of less than 5°, and a gradually curved transition mated the working section with its conical diffuser. The liquid capacity including the pump but excluding the expansion chamber is 10 U.S. gallons.

The tunnel pump-drive system consists of a 15-horsepower, 220-volt, three-phase motor powered through a variable autotransformer and coupled to a centrifugal pump by means of a variable-speed power transmission unit. The pump is made of 356-T6 aluminum and contains an 8.45-inch-diameter three-vaned impeller with splitter vanes. Design rating for the pump is 700-gallon-per-minute flow rate with a total head rise of 250 feet of liquid at 3500 rpm. To avoid possible pump cavitation, the pump is intentionally oversized with respect to design maximum speed of the tunnel and thus does not attain rated conditions. With water as the working fluid and a 1.743-inch cylindrical test section, the drive system provides continuously variable pump speeds from 550 to 2300 rpm. These pump speeds

correspond to water flow velocities in the cylindrical test section from about 19 to 80 feet per second.

The tunnel facility was designed to operate over a pressure range from 0 to 250 pounds per square inch absolute and a temperature range from +140° F to less than -320° F. High-pressure nitrogen gas was normally used as the pressurizing medium. Tunnel pressures less than atmospheric pressure were obtained by means of a vacuum system incorporating absolute pressure regulators for control. Excluding the plastic working section, static pressures were measured in the expansion chamber, across the contraction nozzle (by a manifolded ring of taps in the inlet and outlet flanges), and at pump inlet and outlet flanges. Copper-constantan thermocouples located $4\frac{1}{2}$ inches upstream of the contraction nozzle were used to measure water temperature.

Working Sections

Two different water-tunnel test sections were used. A 1.743-inch constant-diameter section was used to evaluate facility performance and established the degree of flow uniformity at the test section. The cavitation studies were made with a venturi section. The venturi shape was designed to provide a wall-pressure profile with a deep but narrow valley for the attainment of local tension. As shown schematically in figure 2(a), the venturi uses a modified quarter round (nominal radius, 0.183 in.) to provide transition from a 1.743-inch free-stream diameter to a 1.377-inch throat diameter. The 0.75-inch-long throat is followed by a conical diffuser of $4\frac{1}{2}^{\circ}$ total angle.

The water-tunnel test sections were machined from transparent acrylic plastic. The entrance and exit diameters of 1.743 inches were mated to aluminum mounting flanges by a shrink-fit technique. The interference fit required for this operation was 0.002 or 0.003 inch, and the resulting slight taper of the test-section inner bores was considered negligible herein. Precision machining and assembly held all gaps and discontinuities to less than 0.001 inch. Design symmetry allowed the test sections to be rotated in 60° increments about the flow axis or even to be turned end for end as desired.

Instrumentation of the 12-inch-long venturi section consisted of 10 static-pressure taps, located as in figure 2(a), and a manually traversable total-pressure probe mounted in the downstream flange. The taps were carefully and accurately machined perpendicular to the local contour of the previously polished inner wall. Tap openings were then carefully hand polished to remove all evidence of imperfections as determined with magnifying devices and special lighting. Tap diameters were all 0.040 inch except taps 2 and 3 (fig. 2(a)), which were 0.020 inch in diameter. Taps were installed at various circumferential positions to minimize possible downstream interference effects of alined taps. As detailed in figure 2(a), the total-pressure probe was made of stainless steel and consisted of a single Pitot tube mounted in the leading edge of a hollow, streamlined support strut. After polishing, accurate measurements of the venturi profile were made to determine its final contour. A sketch of the water venturi contour along with the contour for an enlarged (4.61 scale) model used for sub-

sequent wind-tunnel checks of pressure distribution is presented in figure 2(b). The nominal design contour, or true quarter round, is shown as a dash-dot line for convenient reference. The water- and wind-tunnel contours, called modified quarter round hereinafter, are practically identical, both differing from a true quarter round mainly in local radius of curvature and in a slight taper in the throat entrance region.

The wind-tunnel simulation of the water-tunnel model is shown schematically in figure 2(c). The constant-diameter approach section of the water-tunnel venturi (fig. 2(a)) was simulated in the aerodynamic model by an 8.03-inch-internal-diameter machined steel pipe with a sharpened leading edge. A precision-turned wooden piece containing the scaled-up modified quarter-round contour (fig. 2(b)) was inserted into the downstream end of the pipe. The conical diffuser was foreshortened for convenience. Free-stream instrumentation (within the approach pipe) consisted of a ring of four static taps drilled through the pipe wall 3.44 inches upstream of the leading edge of the wooden insert. Ten additional static taps were placed within this 3.44-inch interval. Free-stream velocity and velocity distribution within the approach section were determined by means of a total-pressure rake inserted across the pipe radius at the static ring plane. Static-pressure measurements on the contoured wooden insert were obtained by means of a multiple-tube plastic belt drilled to provide 21 strategically spaced pressure taps, each 0.020 inch in diameter. The belt was cemented onto the wooden insert and then measured for tap location. The wind-tunnel model was alined with the airflow in the center of the 6- by 9-foot test section of the Icing Research Tunnel of the Lewis Research Center. With the enlarged aerodynamic model, 11 pressure taps were located on the critical modified quarter-round portion of the venturi, whereas with the water-tunnel model only one tap at 78.4° of arc from the start of the quarter round was feasible.

Except for tap location, instrumentation of the 12-inch-long constant-diameter water-tunnel calibration model was similar to the venturi model. Nine 0.025-inch-diameter taps, about equally spaced, were drilled into the plastic portion of the test section, and one 0.063-inch tap was located in each end flange.

Manometry

Water-tunnel and working-section pressures were measured by banks of 7-foot-high multiple-tube mercury manometers. The sealed mercury reservoirs of the manometers were interconnected with the tunnel pressurization system so that all readings were relative to the tunnel pressure measured in the gas space within the expansion chamber. This reference tunnel pressure was measured by a mercury column when possible, otherwise by a precision gage. Pressure, or piezometer, lines were of transparent plastic tubing, and each contained a bleed valve at the manometer end and an orifice-type restrictor near the tunnel end; the latter feature minimized mercury column oscillation. Manometers were read to within about ±0.025 inch.

Pressures within the aerodynamic venturi model were measured by banks of 10-foot-high multiple-tube water manometers.

Photographic and Sound Equipment

Cavitation was photographed by a still camera (4- by 5-in. film size) in conjunction with a 1.2-microsecond high-intensity flash unit, as well as with a high-speed movie system. The movies (6000 frames/sec max.) were taken by a 16-millimeter high-speed movie camera coupled to a synchronized light source.

A few exploratory noise measurements of cavitation were made employing a sensitive microphone and a two-channel tape recorder. A standard medical stethoscope was routinely used as an aid in detecting audible cavitation.

PROCEDURE

Conditioning of Water Samples

Three types of water were used in the tunnel studies; namely, demineralized, tap, and distilled water. The demineralized water (sometimes called deionized) was obtained from tap water processed through a commercial demineralizer (Barnstead type FM-4), which delivers mineral-free water after an ion-exchange process. Unlike distilled water, demineralized water may retain bacteria, organic impurities, silica, and other nonionizable substances. Tap water was from the municipal water supply of Cleveland, Ohio. Before use, the tap water was passed through standard filter paper (approx. 12-micron pore size) to remove foreign particles such as rust and scale. Comparable filtration of demineralized water was achieved in processing, and no further filtering was done. The distilled water used was commercially available distilled drinking water. It should be noted that the purity of the distilled water, as it existed in the tunnel, is subject to some question. Preliminary studies, involving tap and distilled water, disclosed contamination of the distilled water by some corrosion particles from the tunnel circuit and possible contamination by the tap water previously used. The tunnel was dismantled, cleaned, and dried, but the new supply of distilled water was insufficient to refill the tunnel. The remainder required was provided by paper filtering the contaminated distilled water previously used.

The three water types normally contained at least 16 milligrams of gas (assumed to be normal air herein) per kilogram of water (about 67 percent air-saturated at room temperature) and were generally degassed prior to tunnel use. Air removal was accomplished by boiling in a clean, electrically heated, stainless-steel processing tank at atmospheric pressure. The tank was immediately sealed, and the water was cooled to room temperature for storage from 1 to 3 days before transfer to the tunnel. To minimize contamination by air, the treated water was transferred to the tunnel by a low-pressure technique. The tunnel and fill lines were evacuated to about 0.20 foot of water pressure absolute, the processing tank discharge valve was opened, and a pressure difference of 1 to 6 feet of head delivered water to the tunnel by way of the pump housing (fig. 1(b)). With the tunnel full of water, some free air was always trapped in the region of highest elevation (elbow A, fig. 1(b)). This air was removed in 20 to 30 minutes by venting through the cap of the expansion chamber while tunnel water was circulated at low speed. The air escaped from the free surface in the expansion chamber. The initial sampling of the tunnel water for air-content analysis was made toward the end of this slow circulation phase.

Air Content of Water

A conventional Van Slyke Gas Analyzer (see ref. 5) was used to determine air content. Briefly, the apparatus removes entrained and dissolved gases by a vacuum process and measures their combined partial pressure. From this partial pressure of the removed gases and their volume, weight is determined by assuming the gases to be normal air. Water samples were withdrawn by a pipette inserted to the tunnel centerline through the expansion chamber while the pump was slowly circulating the tunnel water. Generally, the sample was drawn, taken to, and sealed within the readied Van Slyke instrument in less than 30 seconds. Samples from a new charge of tunnel water resulted in values of absolute air content from 1.4 to 3.2 milligrams of air per kilogram of water (about 6 to 13 percent of atmospheric saturation at 70° F). Air-content measurements were made at least at the start and end of each operating day and always after intentional change in air content. After sampling, the tunnel was sealed and pressurized, and all piezometer lines were bled of any air.

Stability of air content during the 2- to 4-hour operating day was such that absolute air content generally increased less than 1.5 milligrams of air per kilogram of water. To cover the program range of air content from about 1.4 to 26.3 milligrams of air per kilogram of water, air was intentionally added for subsequent runs. This was accomplished by adding high-air-content water (generally available from the nonboiled supply) to the tunnel while an equal amount of tunnel water was withdrawn. Tunnel water was renewed at least once a week. Periodically the tunnel was disassembled, and each component was thoroughly washed in a solution of 5 percent acetic acid and 1 percent detergent to maintain cleanliness.

Cavitation Criteria

Incipient cavitation. - As is usual in water-tunnel studies, the degree or amount of cavitation produced on the venturi is controllable. The minimum degree of cavitation, herein termed incipient cavitation, defines an operating point at which the formation and/or collapse of vapor bubbles on or near the model surface becomes just detectable by either visible (eye) or audible (ear) means. This operating point may differ depending on whether the visible or audible criteria are specified. It is realized that the incipient degree of cavitation is somewhat arbitrary in that subaudible or subvisible changes may occur in the water. However, for all practical engineering applications, subaudible or subvisible changes in flowing water do not affect the usual performance parameters such as pump efficiency.

The present study is primarily concerned with vaporous cavitation and not the relatively slow diffusion process of gaseous cavitation wherein degassing may occur from water that is locally supersaturated with air. To avoid or minimize degassing effects, no data are reported where supersaturated conditions, based on tunnel temperature and local static pressure, exist in the free-stream approach section. The degree of saturation was calculated from Henry's law, which states that saturation is directly proportional to local pressure. In general, calculated free-stream supersaturation was confirmed visually in that small bubbles were observed (under strobe lighting) in the stream ahead of the venturi con-

striction. The presence of such bubbles increased the incipient-cavitation parameter K_i (described later) about 5 percent. Occasionally small flecks (possibly bubbles) were observed in the free stream at conditions 10 to 20 percent less than saturation conditions as predicted by Henry's law. These data are presented because they agree with results obtained under conditions of no visible upstream irregularities. For the major portion of all reported data, the free stream ahead of the venturi constriction was less than saturated and visually free of any bubbles or flecks.

In the present study, the occurrence of visible cavitation at incipience was readily defined by the abrupt appearance of numerous and sizable cavities (at least 1/8 in. long) whose leading edges were upstream of the venturi shoulder (i.e., in the region of minimum pressure). A photograph showing typical incipient cavitation is presented in figure 3. A general discussion on the characteristics of cavitation, including degrees of cavitation greater than incipient, is presented later in the section "Observations of Cavitation." Incipient cavitation as defined denotes only the degree of cavitation and not the method by which it was produced. The present study is concerned predominantly with incipient cavitation, although degrees of cavitation greater than incipient were investigated.

Methods of producing incipient cavitation. - Although cavitation on a water-tunnel model can be produced by increasing stream velocity while maintaining a constant overall system pressure, in the present study it was found more convenient to fix velocity and vary the pressure level. (No difference in results was obtained.) Herein, for a particular constant free-stream velocity, incipient cavitation was produced in two ways: (1) by the onset method, and (2) by the suppression method. With the onset method the overall system pressure was gradually reduced until incipient cavitation occurred. With the suppression method, cavitation in excess of incipient conditions was first generated, and then was suppressed or reduced to the incipient state by gradually increasing system pressure. With either visual or audible detection, the onset method resulted in the same system pressure, within the accuracy of measurement, for incipient cavitation as did the suppression method. Thus, for incipient cavitation as defined, no hysteresis effects were observed. Other studies (e.g., ref. 2) have shown definite hysteresis effects in the results obtained between the onset and suppression methods. The onset method was favored herein for convenience, although both methods were often used.

During operation with taps 2 and 3 purposely plugged (fig. 2(b)), the onset method occasionally did not produce visual incipient cavitation as defined. Instead, system pressure could be gradually reduced to lower than usual for incipient cavitation without the appearance of cavitation. A further small pressure reduction would result in the sudden appearance of cavitation far in excess of the incipient degree. This delayed onset produced, as a minimum, a continuous nondisappearing ring of cavitation in the low-pressure region of the venturi. The cavitation ring varied in length from about 3/16 to 1/2 inch, depending on the system pressure level at onset. A photograph showing typical minimal cavitation observed with delayed onset is presented in figure 4. Delayed onset was random, and a repetition usually resulted in incipient cavitation. Suppression of excessive cavitation resulting from the delayed onset cycle would always yield the incipient-cavitation condition. Results from this random phenomena are dis-

cussed later in the section entitled "Supertension."

Visual and audible cavitation detection. - As previously stated, the detection of visible cavitation at incipience is easily defined by the abrupt appearance of sizable vapor cavities in the region of minimum pressure. On the other hand, definition of the audible-incipient-cavitation threshold is difficult because of the subjective criteria used. With the ear or stethoscope (no apparent difference in results) placed firmly against the venturi test section and proceeding with the onset method, audible cavitation was detected initially as distinct but random clicks emanating from the shoulder region. The randomness of these initial clicks (on the order of one every several seconds) indicated the probable collapse of but a few isolated, microscopic cavities and was not considered representative of the bulk of the water under study. A slight further reduction in pressure level produced a nearly steady succession of clicks, and audible incipient cavitation was defined as the condition at which the frequency of clicks (several per second) first became constant. The noise of audible cavitation is believed to be from the sudden collapse of condensing vapor-filled cavities or possibly the collapse of an empty cavity as the cavities enter a relatively high pressure region. Although a small percentage of air may be present in these cavities, it seems unlikely that a predominantly air-filled cavity would audibly collapse because of the relatively long times required for the diffusion process. Visual inspection with aid of strobe lights showed no visible evidence of cavitation anywhere on the model for all degrees of audible cavitation, although viewing at large magnification was not attempted.

An increase in the degree of cavitation from audible incipient to visible incipient produced a corresponding increase in noise intensity with no apparent change of frequency. All observations of cavitation were made by the same person.

Cavitating tap effects. - Tap 2 (fig. 2(b)) was located at the average leading-edge location of visibly observed cavities. Tap 2 measurements of pressure-head coefficient, however, were made only for noncavitating conditions. It was realized that all subsequent venturi cavitation runs would include cavitation at or in the tap, and its effects on the incipient-cavitation threshold would have to be considered. Generally, tap 2 cavitated at all conditions involving pressures less than about 1 foot of water above vapor pressure. Thus, no pressures were measured when the local pressure was near or less than vapor pressure, but were computed as described in the next section.

The effects of tap cavitation on determining incipient-cavitation limit were as follows: Audible incipient detection was not seriously affected by tap 2 cavitation because it was easy to discriminate by ear between the clicks of stream cavitation and the constant hissing sound emanating from the cavitating tap. Cavitating tap 2, however, did affect the sequence of events leading to the determination of visible incipient cavitation. On approaching visible incipient cavitation by the onset method, tap 2 visibly cavitated; then a vaporous cloud spread circumferentially from each side of the tap to include a total arc of about 45°. Incipient visible cavitation was determined when vapor bubbles or voids just occurred at a circumferential location well outside the 45° arc of tap disturbance. The suppression method of producing incipient cavitation yielded identical results in reverse order. The incipient-cavitation results obtained with tap cavitation agreed completely with the limited amount of incipient data

obtained before taps 2 and 3 were installed.

Data Reduction and Presentation

Noncavitating pressure distributions are presented in terms of a nondimensional pressure-head coefficient C_p where

$$C_p \equiv \frac{h_x - h_0}{V_0^2/2g} \tag{1}$$

(All symbols are defined in the appendix.) For the venturi models, free-stream conditions were determined from wall-pressure measurements at an x/D of 1.98 (tap 1 of fig. 2(a) or the static-pressure ring of fig. 2(c)). For the constant-diameter calibration model, free-stream conditions were measured by a wall tap at an x^*/D of zero (midpoint of section). Pressures measured in the water-tunnel models were all corrected to longitudinal centerline values. Pressures measured in the wind-tunnel model were corrected to incompressible values.

Of particular interest on the venturi model are what the noncavitating values of C_p are at the point of minimum pressure $C_{p_{min}}$ and whether the location and values of minimum pressure are the same as those at the leading edge of visibly observed cavities. The location and values of $C_{p_{min}}$ were obtained from aerodynamic measurements on the accurately scaled-up wind-tunnel model (fig. 2(b)), on which it was possible to install numerous pressure taps in the critical region. The location of $C_{p_{min}}$ is constant at an x/D of 2.471 or 66° of arc. To locate a pressure tap at the leading edge of visible cavities, the water-tunnel venturi, initially without taps 2 and 3 installed, was observed under cavitating conditions. Various degrees of visible cavitation were created in the model at several stream velocities, and the leading edge of the cavitation zone was determined by direct measurement and from photographs. The average leading edge of all cavities was approximately constant, occurring at an x/D of 2.492 or about 78° of arc (fig. 2(b)). Following these initial cavitation studies, tap 2 was installed at 78.4°; tap 3 was also installed at this time.

The dynamic flow conditions during cavitation are represented quantitatively by the nondimensional cavitation parameter K where

$$K \equiv \frac{h_0 - h_v}{V_0^2/2g} \tag{2}$$

A body submerged in a flowing liquid has some critical value of K above which the body will operate cavitation-free and below which cavitation is to be expected. The critical K herein is that at which incipient cavitation occurs on the body (walls); for convenience, it is given the symbol K_i:

$$K_i \equiv \left(\frac{h_0 - h_v}{V_0^2/2g} \right)_{\text{incipient}} \tag{3}$$

where, for a given value of V_0, h_0 is measured when incipient cavitation occurs on the model. This, along with h_v determined at the tunnel liquid temperature, allows calculation of K_i. The lower the value of K_i, the more resistive is the body to cavitation. Thus, K_i is a useful index for comparing the susceptibility of various body shapes to incipient cavitation.

A useful relation exists between the incipient-cavitation parameter K_i (eq. (3)) and the noncavitating pressure-head coefficient C_p (eq. (1)). Consider the value of $-C_p$ at the point of minimum pressure; thus,

$$-C_{p_{min}} = \frac{h_0 - h_{min}}{V_0^2/2g} \tag{4}$$

If the flowing liquid cavitates incipiently at vapor pressure, the minimum pressure equals vapor pressure; thus,

$$-C_{p_{min}} = \frac{h_0 - h_{min}}{V_0^2/2g} = \frac{h_0 - h_v}{V_0^2/2g} = K_i \tag{5}$$

Consequently, a measured value of K_i less than $-C_{p_{min}}$ indicates incipient cavitation at a local pressure less than vapor pressure or, as defined herein, a local tensile stress in the liquid. This discussion assumes that the noncavitating values of C_p (including $C_{p_{min}}$) are valid at either audibly or visibly incipient cavitation conditions, since for these conditions only extremely small scale disturbances exist in the flow field. Such disturbances are considered to have a negligible effect on the value of $C_{p_{min}}$, at least for conditions just prior to visible incipient cavitation.

Because at the incipient-cavitation level the minimum pressure on the venturi wall was below vapor pressure and thus could not be measured directly because of the generally cavitating pressure tap, the minimum pressure relative to vapor pressure ($h_{min} - h_v$) was obtained by adding the parameters K_i and $C_{p_{min}}$ (eqs. (3) and (4)); thus,

$$K_i + C_{p_{min}} = \frac{h_0 - h_v}{V_0^2/2g} + \frac{h_{min} - h_0}{V_0^2/2g} = \frac{h_{min} - h_v}{V_0^2/2g} \tag{6}$$

For convenience $K_i + C_{p_{min}}$ is called the local tension parameter, from which the maximum tensile stress, called local tension, becomes

$$h_{min} - h_v = \frac{V_0^2}{2g}\left(K_i + C_{p_{min}}\right) \tag{7}$$

Free-stream velocity V_0 was obtained from the static pressure-head difference Δh across the water-tunnel contraction nozzle (flow coefficient of unity) and design flow area corrections; thus

$$V_0 = 8.12\sqrt{\Delta h} \tag{8}$$

In general, several determinations of visible and audible incipient cavitation were made at each operating condition. The data points presented herein represent one average value of closely repeatable data.

Calibrations

Pressure distributions. - Pressure measurements for the 1.743-inch-constant-diameter, 12-inch-long water-tunnel calibration model are shown in figure 5. In figure 5(a), the axial variation of wall pressure-head coefficient is linear with no significant effect of velocity for the range of Reynolds numbers of 0.33×10^6 to 1.11×10^6 studied. The slope reflects the frictional head loss coefficient that agrees favorably with literature values for smooth circular sections. Figure 5(b) presents total-head profiles across the entrance of the calibration model. These profiles are flat and show no circumferential distortion or variation with Reynolds number. The slight decrease in total head in the immediate vicinity of the wall is indicative of the thin boundary layer present at the working-section entrance. The calibration model results of figure 5 indicated satisfactory water-tunnel flow for subsequent studies of cavitation with the venturi model.

Typical noncavitating axial wall pressure-head coefficients from the water- and wind-tunnel venturi models are presented in figure 6 along with the results from incompressible, irrotational flow computations for the same venturi shape. The water- and wind-tunnel results presented are for a comparable Reynolds number of about 0.46×10^6 (middle of range studied). From figure 6(a), the overall agreement between the experimental pressure-head coefficients for the two models is good. In addition, the solid line representing the results from incompressible, irrotational flow computations at infinite Reynolds number (described later) substantiates the experimental results. The critical low-pressure region is replotted with magnified axial scale on the left half of figure 6(b), while the right half of this figure shows the experimental variation of $C_{p_{min}}$ with Re_D. The close agreement among all results supports the use herein of aerodynamic values of $C_{p_{min}}$, as a function of Re_D, for determination of minimum pressure at incipient-cavitation conditions; $C_{p_{min}}$ varies from -3.20 to -3.43 for an Re_D of 0.23×10^6 to 0.84×10^6, respectively. Over the range of Re_D studied, the value of C_p at an x/D of 2.492 (average leading-edge location of visible cavities) is about 9 percent less negative than $C_{p_{min}}$. The auxiliary water veloc-

ity scale for $C_{p_{min}}$ in figure 6(b) is computed from Re_D using the average water temperature at each test velocity (see tables I and II).

The incompressible, irrotational flow results of figure 6 were determined by the method (relaxation process) detailed in reference 6. Briefly, the results herein were obtained as follows: Values of the axisymmetric or Stokes stream function were determined numerically over a finely divided square network in a representative half plane. Boundary values were assigned to satisfy flow continuity with uniform free-stream velocity assumed at an x/D of 0.403 (2D upstream of nose, fig. 2(b)) and uniform throat-exit velocity at an x/D of 2.953. The square network represented x/D increments of 0.0125 (0.02179 in. on water model). With fixed boundary values and initially assumed interior values, the relaxation process was used to approximate the simultaneous solution of local stream function at over 7000 network intersections. An IBM 7090 computer iterated several hundred times until further iteration yielded no significant change in the local values of the stream function. From derivatives of the stream function at the venturi wall, local to free-stream velocity ratios were obtained from which values of C_p at the wall were computed. These computations ignore the presence of a boundary layer and thus are equivalent to the case of infinite Reynolds number.

The computations as previously described are very sensitive to small changes in body shape and in particular to changes in local radius of curvature. Similar computations were made for a true-quarter-round venturi that differs slightly from the modified water- and wind-tunnel models reported on herein (see fig. 2(b)). Although the computed value of $C_{p_{min}}$ was about -3.80 for the true quarter round, which is almost the same as that shown in figure 6(b), the location of $C_{p_{min}}$ on the true quarter round is near 78° of arc rather than 66° for the modified quarter round. This downstream shift in the location of $C_{p_{min}}$ was confirmed by additional wind-tunnel tests of a true-quarter-round venturi.

The results in figure 6(b) show that C_p decreases sharply from the nose of the modified quarter round to an experimental $C_{p_{min}}$ of about -3.33 (Re_D of 0.468×10^6) at 66° of arc (x/D of 2.471) followed by a sharp rise to a C_p of -1.80 within the throat entrance. The C_p variation just described occurs within a surface distance of less than 0.4 inch. This deep but narrow pressure valley on the venturi wall means that an element of water moving along the wall is exposed but a short time to the low-pressure region.

Exposure times to low pressure. - To illustrate the magnitude of time at low pressure, figure 7 presents absolute static pressure head as a function of axial distance for three free-stream pressures and velocities. These pressure profiles are typical of those associated with visible incipient cavitation. Also indicated are representative values of vapor pressure for each velocity (water temperatures increased with velocity). The total time that the water along the wall is exposed to pressures less than vapor pressure is called exposure time and was calculated from surface distance and average local velocity. From figure 7, ex-

posure time varies from 240 microseconds at a free-stream velocity of 19.5 feet per second to 85 microseconds at V_0 of 44.1 feet per second. Thus, at conditions of visible incipient cavitation, exposure time is almost inversely proportional to free-stream velocity. At visible incipient cavitation, the minimum static pressure head is calculated to be always less than absolute zero; hence, the water on the wall is sustaining a tensile stress. As previously discussed, tensile stress herein is defined as pressure head less than vapor pressure.

RESULTS AND DISCUSSION

Visible Incipient Cavitation

The incipient-cavitation parameter K_i for visible incipient cavitation on the wall of the venturi test section is presented in figure 8 as a function of free-stream velocity. The negative noncavitating minimum pressure-head coefficient $-C_{p_{min}}$ from figure 6(b) is also presented by a dashed curve for convenient reference, as is the computed limit of $-C_{p_{min}}$ at infinite Reynolds number. The K_i values are given for three types of water (demineralized in fig. 8(a); tap and distilled water in fig. 8(b)) and a range of absolute air content η from about 1.4 to 26.3 milligrams of air per kilogram of water. The basic data for visible incipient cavitation are also given in table I.

The demineralized water K_i results in figure 8(a) when cross-plotted show less than a 3-percent effect of air content over the range from 1.4 to 26.3 milligrams of air per kilogram of water (0.06 to 1.11 times atmospheric saturation at 70° F, see table I). Comparison of the demineralized water K_i results with those for tap and distilled water in figure 8(b) indicates little to no effect of water type. At a given air content, the water temperature range from 67° to 110° F (noted in table I) produced no significant effects. The absolute value of K_i increases about 12 percent with velocity from 19 to 45 feet per second and tends to become asymptotic to a value near 2.75.

In figure 8, the visible incipient cavitation parameter K_i is always less than the negative noncavitating minimum pressure-head coefficient $-C_{p_{min}}$, and their difference is approximately constant over the velocity range studied. Values of K_i less than those for $-C_{p_{min}}$ mean (from eq. (5)) that the minimum pressure head on the venturi h_{min} is always less than vapor pressure h_v at the condition of visible incipient cavitation. In fact, from equation (7), the amount that K_i is numerically less than $-C_{p_{min}}$ is a measure of the maximum local tensile stress in the water in terms of velocity head $V_0^2/2g$. The data of figure 8 are replotted in terms of a local tension parameter $(h_{min} - h_v)/(V_0^2/2g)$ and local tension $(h_{min} - h_v)$ in figure 9. For demineralized water (fig. 9(a)), the local tension parameter varies between -0.70 and -0.85. Thus, a reasonable overall approximation of local tension at visible incipient cavitation is that it

equals 75 percent of the free-stream velocity head for the model and range of conditions tested herein. The computed $-C_{p_{min}}$ of 3.82 (at Re_D of ∞) and a K_i value of 2.75 would indicate a maximum local tension parameter of about -1.07 as V_0 approaches infinity. In terms of absolute values of local tension (also presented in fig. 9(a)), the largest value of tension obtained at visible incipient cavitation was about 23 feet of water occurring at a free-stream velocity of 45 feet per second. Tension of approximately 5 feet of water was obtained at the lowest velocity studied (about 20 ft/sec).

During the time the flowing water was locally below vapor pressure, the amount of tension varied from zero to the maximum values presented herein, $h_{min} - h_v$. These exposure times at visible incipient cavitation are plotted for reference across the bottom of figure 9(a) and were determined as follows: For a given V_0, a value of K_i is obtained from figure 8; $-K_i$ is then superimposed across the experimental noncavitating C_p distribution for the appropriate Re_D (see fig. 6(b)), which results in two intersections defining the distance along the venturi side wall that the local pressure is less than the vapor pressure. This distance divided by the average local velocity within it (calculated from average C_p and given V_0) yields exposure time. From figure 9(a) exposure time decreases from about 230 microseconds at a V_0 of 20 feet per second to about 85 microseconds at a V_0 of 45 feet per second. Because vaporous cavitation theoretically occurs only during the exposure time interval, exposure time may prove to be a useful correlating factor when sufficient systematically obtained data for other models and operating conditions are available.

Because water type shows little effect on visible incipient cavitation, the previous discussion concerning local tension and local tension parameter with demineralized water also applies to the tap- and distilled-water results presented in figure 9(b). The visible incipient cavitation results for distilled water are believed valid in spite of the possible contamination of that water type previously discussed (see PROCEDURE).

Supertension. - For purposes of rechecking the effect, if any, of tap cavitation on the determination of visible-incipient-cavitation level, pressure taps 2 and 3 were plugged. Random occurrences of delayed onset of visible cavitation were then observed wherein the maximum tensile stresses averaged about 12 percent greater than those presented in figure 9. These higher values of tension, presented in figure 10, are termed "supertension" and occurred only in the absence of tap cavitation and only for air contents less than 11.0 milligrams of air per kilogram of water. After plugging the taps, about 20 percent of the data obtained at low air content yielded supertension values. Because of their infrequent occurrence and modest effect on maximum tensile stress of the water, the supertension results herein are not considered particularly significant. When supertension occurred, cavitation onset was abrupt, and the initial degree of cavitation exceeded incipient conditions. Suppression to the incipient state, as previously discussed in PROCEDURE, resulted in K_i or local tension values equal to those shown in figures 8 and 9, respectively. The available supertension data of figure 10 do not indicate any marked difference between demineralized and tap

water and no air-content effect for η less than 11 milligrams of air per kilogram of water.

Audible Incipient Cavitation

The audible-incipient-cavitation data are presented in the same way as the visible incipient data just discussed; that is, figures 11 and 12 show, respectively, the incipient-cavitation parameter K_i and local tension as a function of velocity for the three water types over a range of air contents. The basic audible data are also given in table II.

For demineralized water at the lowest air content ($0 < \eta < 5$ mg air/kg water), K_i for audible incipient cavitation (fig. 11(a)) is the same as the visible incipient limit obtained for all water types and air contents. The resulting local tensions and exposure times are likewise the same as shown in figure 12(a). For all water types with air content greater than 5 milligrams of air per kilogram of water, K_i audible generally increases with decreasing stream velocity and also increases with air content. Local tensions at audible incipient cavitation are correspondingly less than those at visible inception. For audible cavitation of demineralized water at a free-stream velocity of 32.5 feet per second, the local tension (fig. 12(a)) is reduced from about 11.4 to 5.8 feet of water as the absolute air content is increased from about 3 to 23 milligrams of air per kilogram of water. For low-air-content tap water (fig. 12(b)) the maximum local tension at audible incipient cavitation is about 60 percent of the value obtained by the visible incipient criteria (21.5 ft water). At high air content and low velocity all three water types audibly cavitated at pressures near vapor pressure ($K_i \cong -C_{p_{min}}$) with consequent little or no tension.

The K_i audible for all tap water in figure 11(b) is considerably higher than K_i visible and shows less effect of stream velocity. The few data points for distilled water (fig. 11(b)) are only at high air content, but these indicate that distilled water is just slightly more resistant to audible incipient cavitation than is tap water. However, the possible contamination of distilled water may have reduced its resistance to audible cavitation.

Exposure times are not plotted in figure 12 for audible incipient cavitation for air contents greater than 5 milligrams of air per kilogram of water because they vary with air content and are rather insensitive to free-stream velocity. In general, exposure times at high-air-content audible cavitation are shorter than at visible cavitation and decrease with air content. Over the range of conditions and water types studied, audible exposure times range between 50 and 130 microseconds for air contents greater than 5 milligrams of air per kilogram of water; whereas, for visible cavitation, exposure times were between 80 and 240 microseconds for all conditions and waters studied (fig. 9(a)).

Effect of Cavitation on Downstream Total Pressure Head

Total-pressure-head measurements were made at the venturi test-section exit

for various degrees of visible cavitation. These results, presented in figure 13, show the ratio of local to centerline total head $H/H_{\text{℄}}$ plotted in terms of radius ratio r/r_T. The measured total-head profiles for noncavitating flow at two values of Reynolds number are presented in figure 13(a). The results obtained for various degrees of cavitation (noncavitating and 0.75- and 2.0-inch cavity lengths) are presented in figure 13(b) for a nearly constant value of Reynolds number. These total-head profiles were measured in the vertical plane only but have been corrected for the relatively small hydrostatic pressure head across the 1.743-inch-diameter exit section and are considered representative for all planes containing the flow axis. The noncavitating results of figure 13(a) show that both total-head profiles are uniform for the inner two-thirds of the exit diameter. The profiles over the remaining portion of the diameter are nearly symmetric with a slight decrease in total pressure shown for the higher Reynolds number. The ratio of area average total pressure head (across the full exit diameter) to centerline total pressure head, $H_{av}/H_{\text{℄}}$, indicates about a 1-percent loss through the venturi test section for noncavitating conditions over the range of Reynolds numbers studied. With increasing degree of cavitation (increasing axial length of cavity), figure 13(b) indicates an average total-pressure-head loss of about 3 and 4 percent, respectively, for the 0.75- and 2.0-inch cavity lengths. Photographs showing the degrees of cavitation associated with the 3- and 4-percent loss in total pressure are presented in figure 14. The percentage loss in total pressure due to cavitation remains small because its disturbance is confined to a narrow ring adjacent to the venturi walls. Even at the test-section exit, which is $7\frac{1}{2}$ inches downstream of the leading edge of the 0.75- and 2.0-inch-long cavities, the cavitation disturbance penetrates into the flow no more than half the exit radius of the venturi. In the plane of measurement, various degrees of cavitation produced no marked asymmetry in total-head profiles.

For reference, the value of the cavitation parameter K is given in figures 13(b), 14(a), and 14(b), where K defines the flow conditions for degrees of cavitation exceeding incipience. A reduction in K from the incipient value of 2.62 (associated with cavity length of zero) to a K of 2.33 produces a 0.75-inch cavity length, and a K of about 2.31 results in a 2.0-inch cavity. This latter sensitivity of cavity length with K is due to the relatively flat pressure-head distribution through the throat and diffuser of the venturi as indicated in figure 6(a).

Observations of Cavitation

Cavitation was always confined to a thin ring of vapor pockets adjacent to the wall, and in all cases the average leading edge was located at or near the 78° location (fig. 2(b)). Thus, there is evidence of a time or distance delay between the location at which vapor cavities may have originated (minimum pressure location of 66°) and the location at which the cavity leading edge was visible. Visible cavitation was of the fixed, rather than traveling type. As described in reference 7 and observed herein, fixed cavities are very irregular in shape; portions of the cavities appear to be entrained by the flowing stream and swept downstream; and collapse, entrainment, and disappearance occur in regions where pressure is above vapor pressure. A traveling cavity is generally

spherical, growing and collapsing several times during its passage downstream from the minimum pressure region; none of these features were seen. Venturi cavitation was unsteady for all degrees of cavitation and free-stream velocities studied, as evidenced by random fluctuations in cavity length and circumferential position at a fixed flow condition. In general, cavitation was more unsteady as the degree of cavitation was increased and was particularly pronounced when the collapsing zone of cavitation occurred in the venturi diffuser.

Visible incipient cavitation always occurred as a practically instantaneous burst of elongated vapor pockets readily detectable both visibly and audibly (fig. 3). The physical character of visible cavitation at inception varied somewhat with air content and to a lesser extent with stream velocity. At low air content ($\eta < 5$ mg air/kg water), incipient cavitation apparently originated at a single point but immediately spread circumferentially to include an angle as much as 90° before disappearance. Each burst, which lasted a few milliseconds at most, would generally be followed by several seconds of cavity-free operation before another burst, usually originating in a different circumferential position, occurred. As air content was increased, the frequency of incipient-cavitation bursts increased, and the circumferential spread of each burst decreased. Near air saturation, the incipient cavitation consisted of many small bursts rapidly occurring about the periphery of the throat entrance. At the higher air contents, visible incipient cavitation was accompanied by rather loud rattling noise, whereas at low air contents there was very little noise. Similarly, audible cavitation at conditions just prior to visible incipience was noisier with water of high-, compared with low-air content. It is postulated that, for conditions just prior to visible incipience, the size of the collapsing cavities was larger for water having the higher air content. If so, more noise is to be expected at conditions just prior to visible inception with high-, compared with low-air content water.

At fixed air content but increased stream velocity, the visible incipient cavity length decreased, reflecting the steeper adverse pressure gradient at the higher velocity (fig. 7). The steeper gradient increased the rate of cavity collapse and thus reduced cavity length. Because of the narrow pressure valley (fig. 6), the change in incipient cavity length with stream velocity was small, varying from about 3/16 inch at 20 feet per second to slightly less than 1/8 inch at 40 feet per second. The trailing edge of even the shortest visible cavity extended about 1/16 inch into the venturi throat.

A small reduction in free-stream static pressure from incipient conditions (0.4 to 1.2 ft of water at low and high speeds, respectively) produced a complete nondisappearing ring of cavitation (fig. 4) 3/16 to 5/16 inch long. This cavitation ring is composed of many individual vapor pockets or streamers whose rates of formation and collapse are very rapid. Motion pictures taken at 6000 frames per second proved to be several times too slow to describe adequately the mechanism of cavitation. Occasionally, a short movie sequence showing the collapse history of a single cavity was obtained, but the history of formation was never apparent, indicating that, for the fixed-type cavities on the model studied, the rate of formation of a cavity may be considerably greater than its rate of collapse. Strips of typical high-speed movies (5640 frames/sec) showing closeups of the leading edge of cavitation are presented in figure 15. The movies shown are for ring cavitation of 1/4-inch length (comparable to that presented in

fig. 4). Figure 15(a) shows the history and collapse of a single cavity for a total elapsed time of about 0.001 second (six frames), while figure 15(b) follows the collapse of a cavity for about 0.0005 second. In both instances, the movie frame immediately following the collapse of one cavity shows a new well-developed cavity already formed.

In general, the high-speed movies obtained near incipient conditions show that the cavitation phenomena have no apparent order as to cavity shape, overall size and width of the individual cavities, or frequency of occurrence at a point location. At the same tunnel speed, the leading edge of a vapor cavity is more rounded, the cavity width greater, and the total number of cavities (streamers) less for smaller degrees of cavitation (figs. 3, 4, and 15) than for large amounts of cavitation (fig. 14(b)). The surface at the vapor-water interface of a cavity was irregular and at times consisted almost entirely of waves that extended from just downstream of the leading edge to the zone of collapse. For the most part, cavity edges had a very ragged appearance. The trailing-edge region of cavitation was extremely irregular because of the violent nature of the collapsing process.

Regions of separated or reversed flow occurred in the venturi diffuser for cavitation lengths exceeding about 1.5 inches. These zones of separation were uniformly spaced about the diffuser periphery (see fig. 14(b)) and increased in number with increasing degree of cavitation. Separation was apparently initiated at the throat-diffuser juncture.

Limited cavitation noise data obtained by a microphone mounted near the outside wall of the venturi were recorded for various degrees of visible cavitation at a constant free-stream velocity of 28.8 feet per second, an air content of 7.6 milligrams of air per kilogram of water, and with demineralized water. Frequency spectrum analyses of these data, when compared with a spectrum analysis of tunnel background noise, yield a measure of the noise generated by cavitation, at least in the range where noise due to cavitation exceeds background noise either in frequency or energy level. The results show that, for the degrees of cavitation studied (0.25- to 2.25-in. lengths), the noise generated by cavitation included frequencies to at least 25,000 cps. It is very probable that higher frequencies existed, but, because of the frequency response characteristics of the equipment and sound transmission losses through the air and model wall, these higher frequencies were not recorded. Comparisons of energy levels existing at the various frequencies could not be made, since frequencies present far exceeded the flat response range (approx. 12,000 cps) of the sound equipment used.

It is interesting to note that, although exposed to visible cavitation for many hours under a variety of conditions, the acrylic plastic venturi suffered no apparent cavitation damage.

SUMMARY OF RESULTS

Studies of cavitation induced on the wall of a venturi in a small water tunnel using demineralized, tap, and distilled water over a range of air content, pressure, and speed yielded the following principal results:

1. Local minimum wall pressures always significantly less than vapor pressure were obtained at visible incipient cavitation of demineralized, tap, or distilled water. The local tensile stresses ranged from 5 to 23 feet of water irrespective of water type or air content and increased with speed.

2. The tensile stresses at audible incipient cavitation were, in general, less than at the visible threshold except for low-air-content demineralized water where the results were the same. At audible incipient cavitation, tensile stresses approached zero at low speed and high air content.

3. Total-pressure losses caused by visible cavitation were about 1 percent at inception, increasing to 4 percent with a 2.0-inch cavity length.

4. Visible incipient cavitation was of the fixed type and always occurred as a practically instantaneous burst of vapor pockets in the region of minimum pressure.

5. Venturi cavitation was unsteady for all degrees of cavitation and stream velocities studied.

Lewis Research Center
National Aeronautics and Space Administration
Cleveland, Ohio, November 7, 1962

APPENDIX - SYMBOLS

C_p	pressure-head coefficient, $(h_x - h_0)/(V_0^2/2g)$, dimensionless
$C_{p_{min}}$	minimum pressure-head coefficient, $(h_{min} - h_0)/(V_0^2/2g)$, dimensionless
D	free-stream diameter, 1.743 in. for water models; 8.03 in. for aerodynamic model
g	acceleration due to gravity, 32.2 ft/sec^2
$H/H_{\text{℄}}$	ratio of local to centerline total pressure head, dimensionless
$H_{av}/H_{\text{℄}}$	ratio of area average total pressure head to centerline total pressure head, dimensionless
Δh	static-pressure-head difference across tunnel contraction nozzle, ft water
h_{min}	minimum static pressure head, ft water abs
h_0	free-stream static pressure head at x/D of 1.98 or x*/D of 0, ft water abs
h_v	vapor pressure head corresponding to water temperature, ft water abs
h_x	static pressure head at x/D, ft water abs
h_{x^*}	static pressure head at x*/D, ft water abs
K	cavitation parameter, $(h_0 - h_v)/(V_0^2/2g)$, dimensionless
K_i	incipient-cavitation parameter, $[(h_0 - h_v)/(V_0^2/2g)]_{incipient}$, dimensionless
Re_D	free-stream Reynolds number with diameter D, dimensionless
r/r_T	ratio of local to full-stream radius (r_T = 0.8715 in.), dimensionless
V_0	free-stream velocity at x/D of 1.98 or x*/D of 0, ft/sec
x	axial distance from venturi model entrance, in. (see fig. 2)
x*	axial distance from midpoint of calibration model, in.
η	absolute air content by weight, mg air/kg water

REFERENCES

1. Numachi, Fukusaburo: The Effect of Air Content on the Appearance of Cavitation in Distilled, Salt, and Sea Water. Trans. and Commentary, Ordnance Res. Lab., Penn. State College, Aug. 1, 1946.

2. Kermeen, R. W., McGraw, J. T., and Parkin, B. R.: Mechanism of Cavitation Inception and the Related Scale-Effects Problem. Trans. ASME, vol. 77, no. 4, May 1955, pp. 533-541.

3. Williams, E. E., and McNulty, P.: Some Factors Affecting the Inception of Cavitation. Cavitation in Hydrodynamics - Proc. of Symposium, Nat. Phys. Lab., Sept. 14-17, 1955.

4. Ziegler, G.: Tensile Stresses in Flowing Water. Cavitation in Hydrodynamics - Proc. of Symposium, Nat. Phys. Lab., Sept. 14-17, 1955.

5. Crump, S. F.: Determination of Critical Pressures for the Inception of Cavitation in Fresh and Sea Water as Influenced by Air Content of the Water. Rep. 575, David W. Taylor Model Basin, Oct. 1949.

6. McNown, John S., Yih, Chia-Shun, and Hsu, En-Yun: Applications of the Relaxation Technique in Fluid Mechanics. Trans. Am. Soc. Civil Eng., vol. 120, 1955, pp. 650-686.

7. Knapp, Robert T.: Cavitation Mechanics and Its Relation to the Design of Hydraulic Equipment. Proc. Inst. Mech. Eng. (London), ser. A, vol. 166, Apr. 1952, pp. 150-163.

TABLE I. - VISIBLE INCIPIENT CAVITATION

Data point number	Absolute air content, η, $\frac{\text{mg air}}{\text{kg water}}$	Tunnel water temperature, $^{\circ}F$	Free-stream static pressure head at incipient cavitation, h_0, ft water abs	Free-stream average velocity, V_0, ft/sec	Data point number	Absolute air content, η, $\frac{\text{mg air}}{\text{kg water}}$	Tunnel water temperature, $^{\circ}F$	Free-stream static pressure head at incipient cavitation, h_0, ft water abs	Free-stream average velocity, V_0, ft/sec
Demineralized water									
1	12.0	90	31.33	27.15	42	16.3	79	35.39	28.95
2	7.0	77	30.23	27.15	43	17.9	89	59.11	37.16
3	5.0	73	42.98	32.46	44	17.9	102	84.31	44.25
4	5.0	83	15.90	19.83	45	26.3	96	59.10	36.97
5	9.2	82	59.68	37.56	46	26.3	108	84.53	44.20
6	8.6	89	34.92	28.61	47	1.4	78	21.92	23.11
7	8.8	96	36.25	28.87	48	1.7	83	15.64	19.52
8	10.0	75	35.57	28.97	49	1.8	76	15.16	19.37
9	11.4	96	55.64	35.82	50	2.3	74	15.16	19.48
10	5.5	68	35.08	28.92	51	2.8	77	34.62	28.70
11	4.9	69	34.36	28.77	52	3.9	75	21.62	22.96
[a]12	4.9	78	32.59	28.89	53	3.9	82	58.87	37.09
13	4.9	78	34.65	28.89	54	4.0	95	83.26	44.05
14	4.5	67	35.10	28.83	55	22.1	76	35.30	28.70
15	6.4	74	15.59	19.71	56	22.1	88	59.40	37.00
16	6.7	83	28.02	25.88	57	24.2	100	83.84	44.03
17	6.7	75	41.93	31.72	58	3.2	82	35.75	29.11
18	7.6	82	59.92	37.52	[a]59	3.2	86	32.80	29.11
19	8.0	81	35.42	28.98	60	3.2	82	35.21	28.97
20	11.6	84	35.36	28.91	[a]61	3.2	87	32.83	29.21
21	13.9	80	35.67	28.98	62	3.7	86	35.84	29.17
22	16.3	88	36.33	28.94	[a]63	3.7	86	33.79	29.13
23	19.2	85	36.37	28.91	[a]64	3.7	84	21.44	23.32
24	21.8	87	36.81	28.90	65	3.7	85	22.64	23.30
25	3.6	86	35.54	28.92	66	4.8	88	59.17	37.26
26	4.5	88	15.87	19.54	[a]67	4.8	90	56.67	37.26
27	5.0	94	59.34	37.26	68	4.8	102	83.78	44.14
28	6.1	101	88.27	45.28	69	11.3	93	35.99	28.86
29	2.5	83	35.14	28.82	[a]70	11.3	96	34.90	28.97
30	2.8	83	15.34	19.49	71	11.3	96	23.07	23.14
31	2.8	79	15.27	19.44	72	11.3	82	35.41	29.05
32	3.7	82	20.71	22.36	73	11.3	91	59.09	37.14
33	4.1	92	70.49	40.51	[a]74	11.3	87	56.80	37.09
34	5.7	75	15.16	19.36	[a]75	11.3	97	82.25	44.08
35	5.7	81	34.89	28.92	76	11.3	101	83.41	43.96
36	6.4	90	58.62	37.00	77	18.8	83	35.24	28.88
37	6.4	101	82.97	43.96	78	18.8	85	35.82	29.04
38	9.6	78	15.18	19.37	79	18.8	90	59.43	37.25
39	9.6	86	34.76	28.65	80	18.8	98	83.18	43.98
40	9.8	88	58.64	37.04	81	18.8	83	59.28	37.26
41	9.8	100	83.24	43.98	82	18.8	91	83.19	43.96
Tap water									
[a]83	2.4	82	35.58	28.95	93	4.1	99	23.25	23.38
[a]84	2.4	86	33.88	29.09	94	11.4	88	35.70	29.03
85	2.4	86	22.61	23.22	95	11.4	88	35.80	29.12
[a]86	2.4	86	21.87	23.25	96	11.4	91	22.78	23.28
87	4.1	86	59.55	37.34	97	11.4	94	59.53	37.20
[a]88	4.1	91	57.82	37.26	98	11.4	89	84.24	44.07
89	4.1	101	85.01	44.31	99	17.9	88	36.03	29.20
90	4.1	98	59.82	37.30	100	17.9	100	60.37	37.16
91	4.1	99	84.37	44.06	101	17.9	106	86.29	44.34
92	4.1	101	36.30	29.12					
Distilled water									
102	1.4	80	35.07	28.86	108	11.0	83	21.69	22.80
103	1.5	86	35.06	28.75	109	11.0	89	58.72	36.92
104	2.8	85	34.82	28.78	110	21.6	81	35.77	29.09
105	9.7	84	34.98	28.79	111	21.6	96	60.11	37.20
106	9.7	86	21.83	22.80	112	21.6	110	85.67	44.12
107	11.0	80	34.83	28.74					

[a]Supertension.

TABLE II. - AUDIBLE INCIPIENT CAVITATION

Data point number	Absolute air content, η, mg air / kg water	Tunnel water temperature, °F	Free-stream static pressure head at incipient cavitation, h_o, ft water abs	Free-stream average velocity, V_o, ft/sec	Data point number	Absolute air content, η, mg air / kg water	Tunnel water temperature, °F	Free-stream static pressure head at incipient cavitation, h_o, ft water abs	Free-stream average velocity, V_o, ft/sec
Demineralized water									
113	10.0	72	38.29	28.97	138	17.9	92	61.41	37.16
114	11.4	93	61.31	35.82	139	17.9	102	84.31	44.25
115	5.5	67	37.65	28.92	140	26.3	94	63.33	36.91
116	6.4	73	17.69	19.71	141	26.3	96	87.75	44.07
117	6.7	72	45.42	31.72	142	1.4	78	22.26	23.11
118	7.6	78	62.33	37.60	143	1.7	82	15.87	19.52
119	13.9	78	38.57	28.91	144	1.8	77	15.39	19.37
120	16.3	86	40.18	28.91	145	3.9	75	21.71	22.96
121	19.2	82	40.88	28.97	146	3.9	82	58.87	37.09
122	3.6	85	36.16	28.98	147	4.0	95	83.26	44.05
123	5.0	94	59.34	37.26	148	22.1	78	40.85	28.70
124	2.5	83	35.14	28.82	149	22.1	92	62.72	36.97
125	2.8	83	15.34	19.49	150	3.7	86	35.84	29.17
126	2.8	78	15.45	19.44	151	3.7	86	22.80	23.30
127	3.7	82	21.56	22.35	152	4.8	88	59.17	37.26
128	4.1	92	70.49	40.51	153	4.8	102	83.78	44.14
129	5.7	75	17.12	19.36	154	11.3	91	37.64	28.91
130	5.7	81	35.86	28.79	155	11.3	96	26.92	23.14
131	6.4	90	58.62	37.00	156	11.3	83	38.00	29.05
132	6.4	101	82.97	43.96	157	11.3	105	84.41	43.96
133	9.6	77	17.54	19.29	158	18.8	82	39.19	28.87
134	9.6	85	35.79	28.80	159	18.8	84	40.00	29.04
135	9.8	88	58.64	37.04	160	18.8	82	64.20	37.20
136	9.8	100	83.24	43.98	161	18.8	90	87.34	43.96
137	16.3	80	39.52	28.95					
Tap water									
162	2.4	81	38.97	28.92	172	4.1	99	28.07	23.38
163	2.4	84	40.41	29.13	173	11.4	86	43.69	29.09
164	2.4	85	26.99	23.28	174	11.4	91	28.64	23.24
165	4.1	89	67.54	37.26	175	11.4	89	69.69	37.26
166	4.1	99	93.31	44.31	176	11.4	98	97.82	44.07
167	4.1	97	69.40	37.50	177	17.9	87	45.18	29.17
168	4.1	105	69.59	37.29	178	17.9	94	71.18	37.25
169	4.1	105	96.59	44.24	179	17.9	102	98.81	44.38
170	4.1	100	42.60	29.12					
171	4.1	93	68.03	37.50					
Distilled water									
180	21.6	79	41.84	28.97	182	21.6	92	69.61	37.26
181	21.6	82	42.33	29.04	183	21.6	106	97.57	44.00

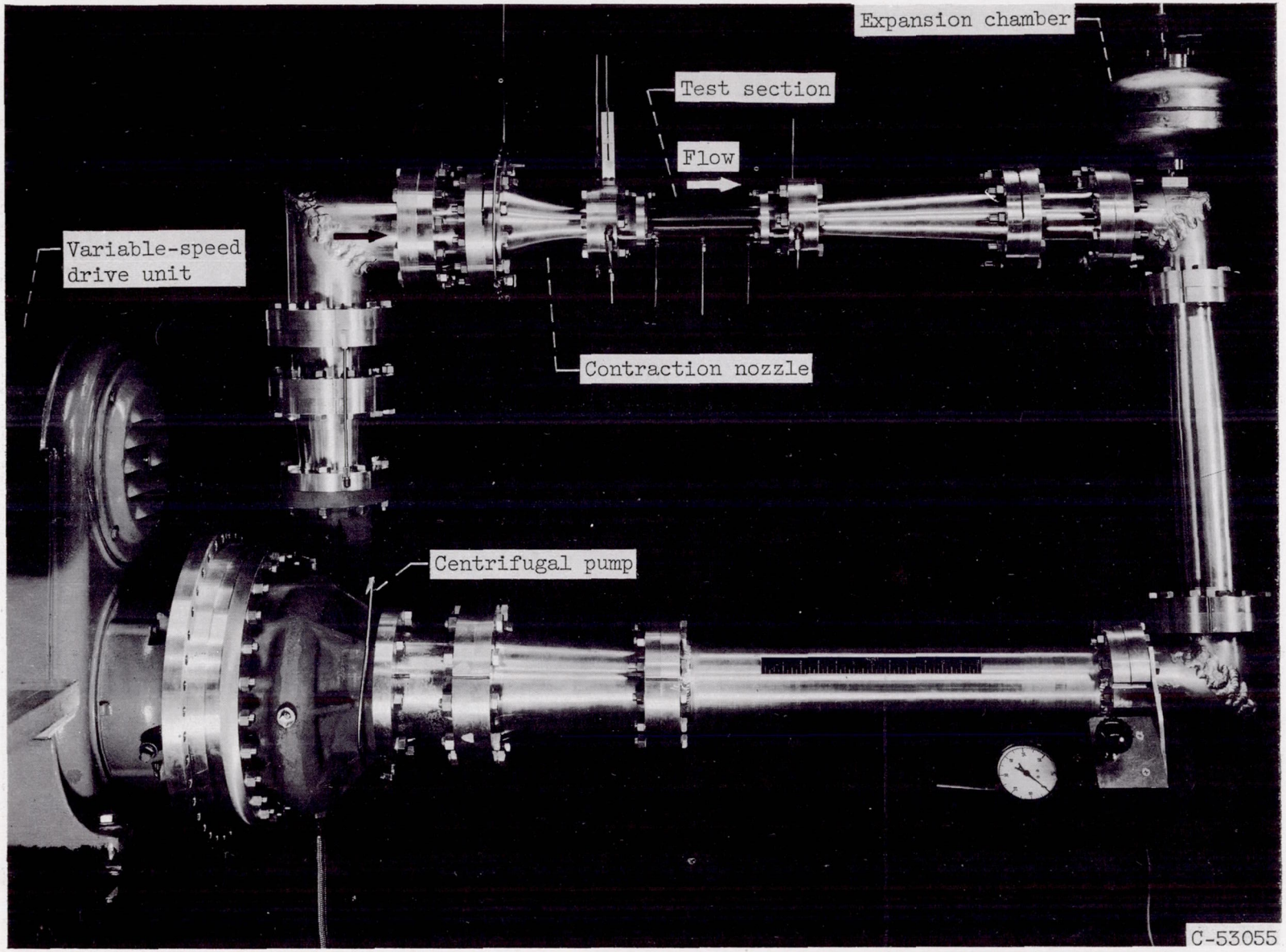

(a) Tunnel loop with partial instrumentation.

Figure 1. - Closed-return tunnel facility.

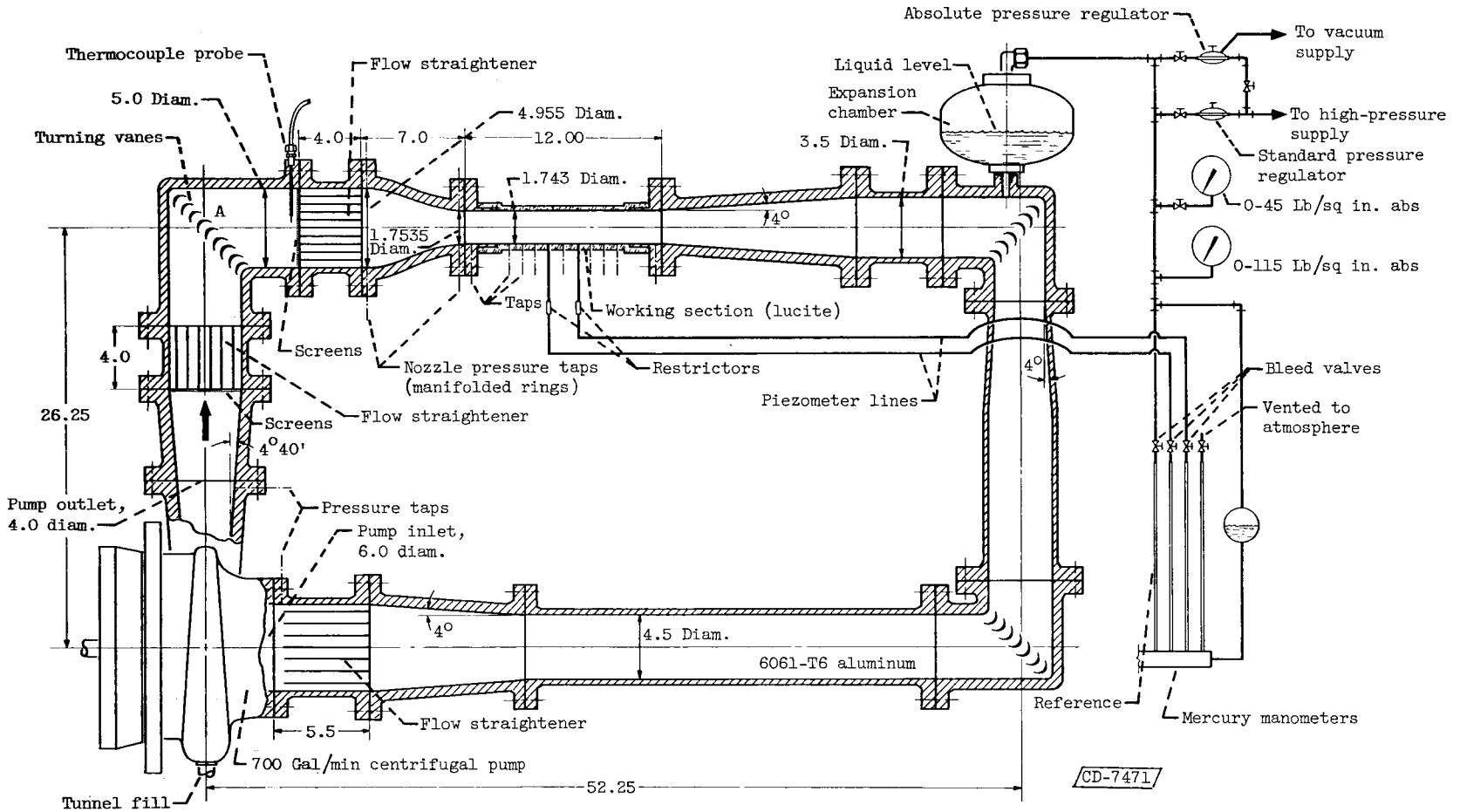

(b) Overall schematic drawing including tunnel pressurization and pressure measurement systems. (Dimensions in inches except where noted.)

Figure 1. - Concluded. Closed-return tunnel facility.

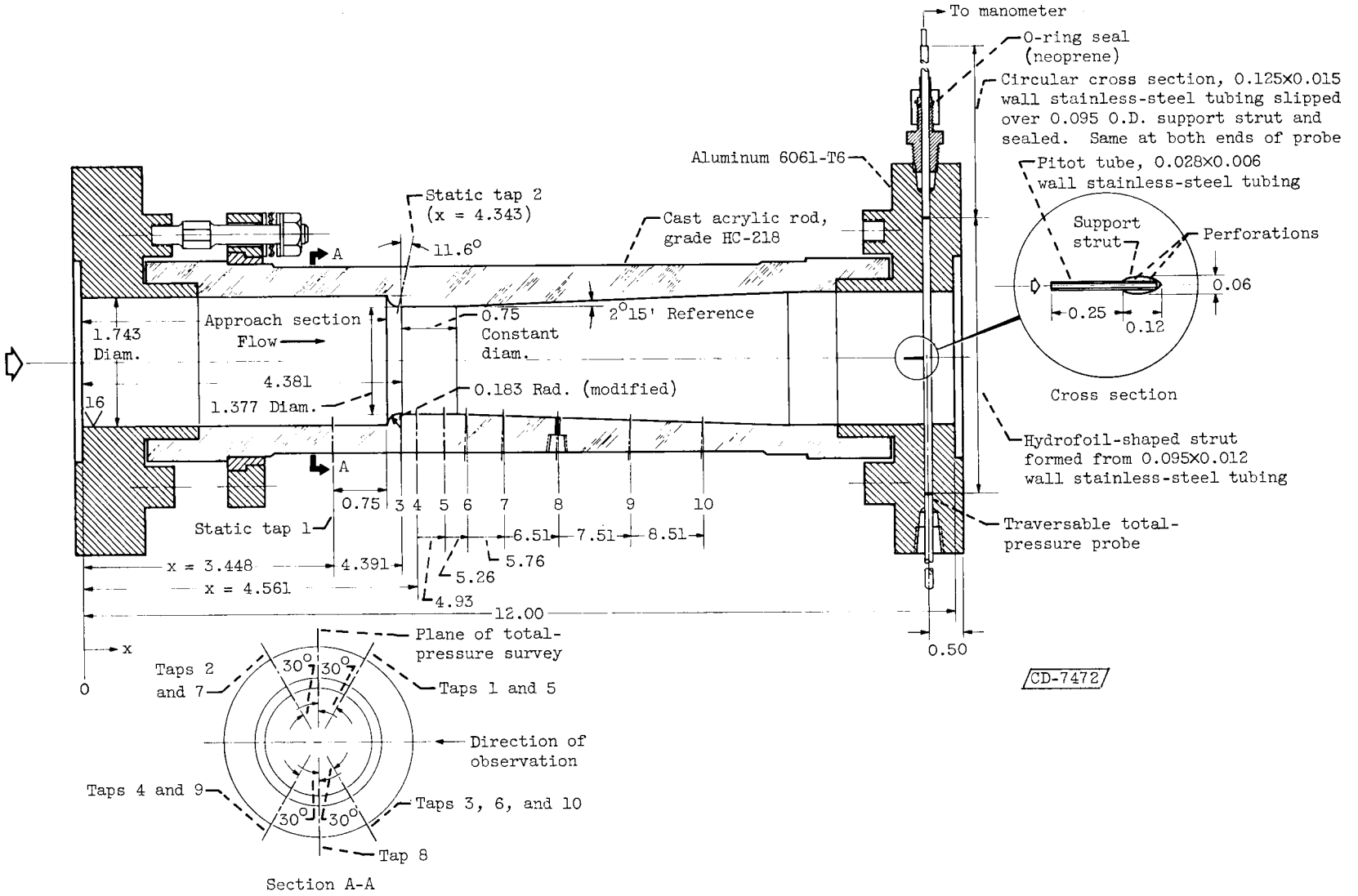

(a) Water-tunnel test section. (Dimensions in inches except where noted.)

Figure 2. - Venturi test sections showing dimensions and instrumentation.

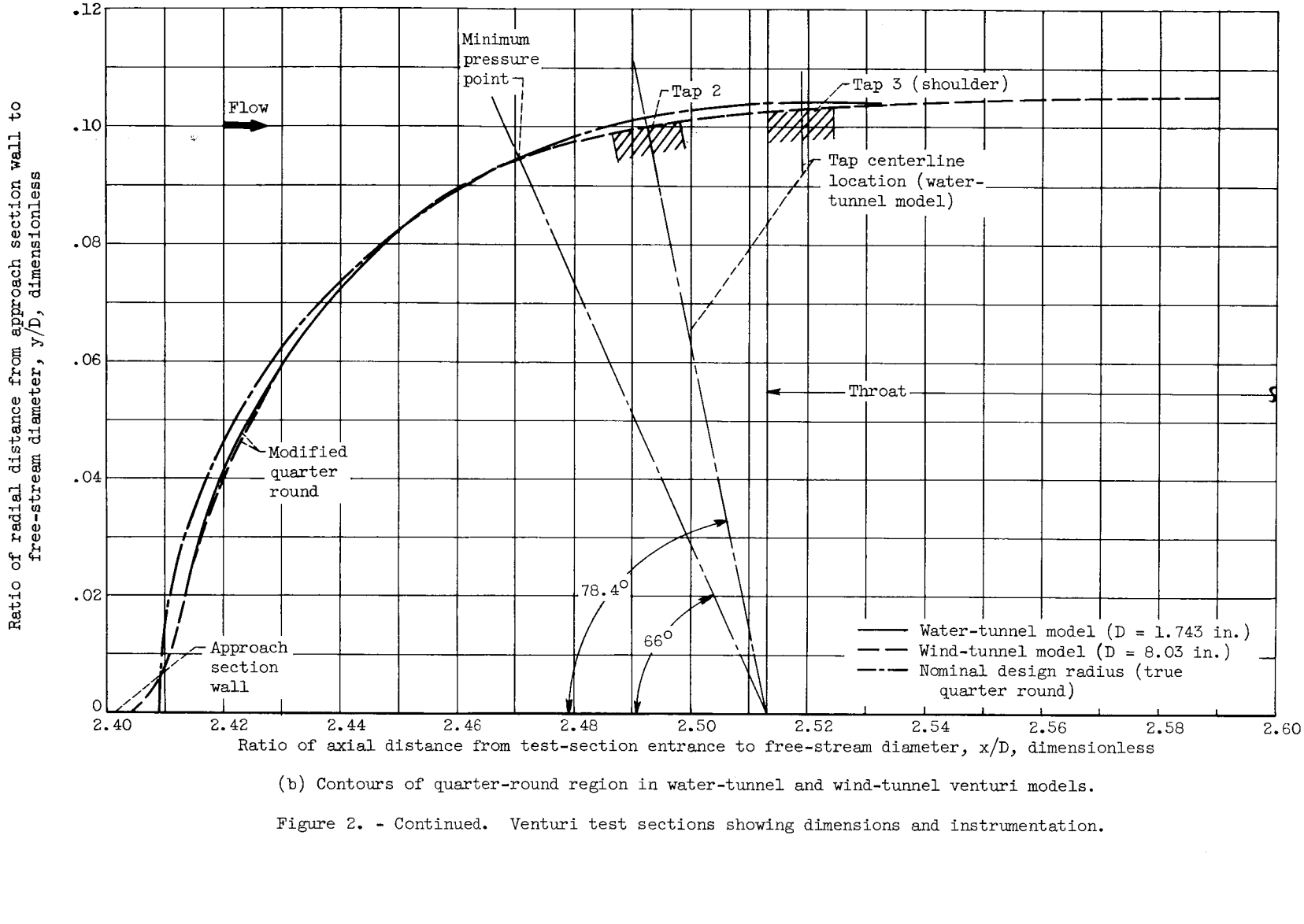

(b) Contours of quarter-round region in water-tunnel and wind-tunnel venturi models.

Figure 2. - Continued. Venturi test sections showing dimensions and instrumentation.

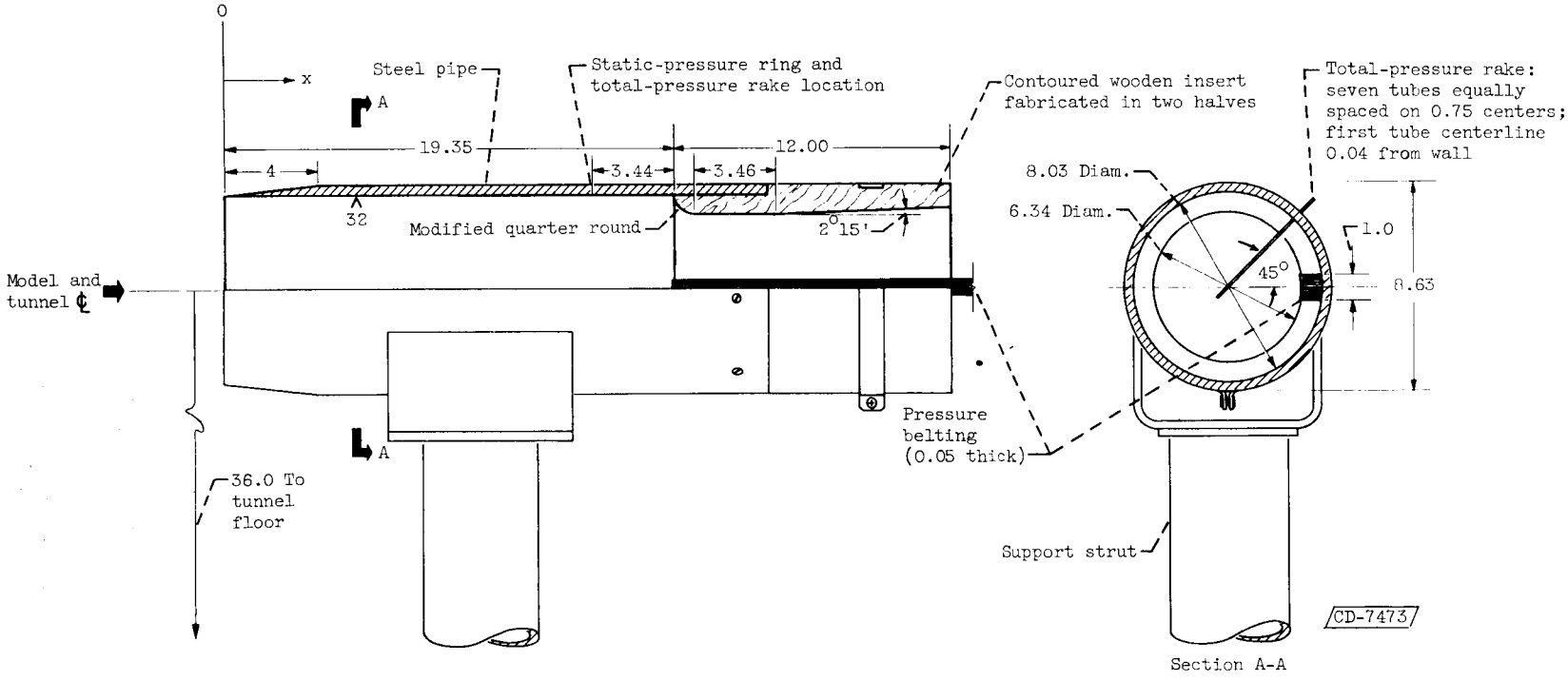

(c) Wind-tunnel model. (Dimensions in inches except where noted.)

Figure 2. - Concluded. Venturi test sections showing dimensions and instrumentation.

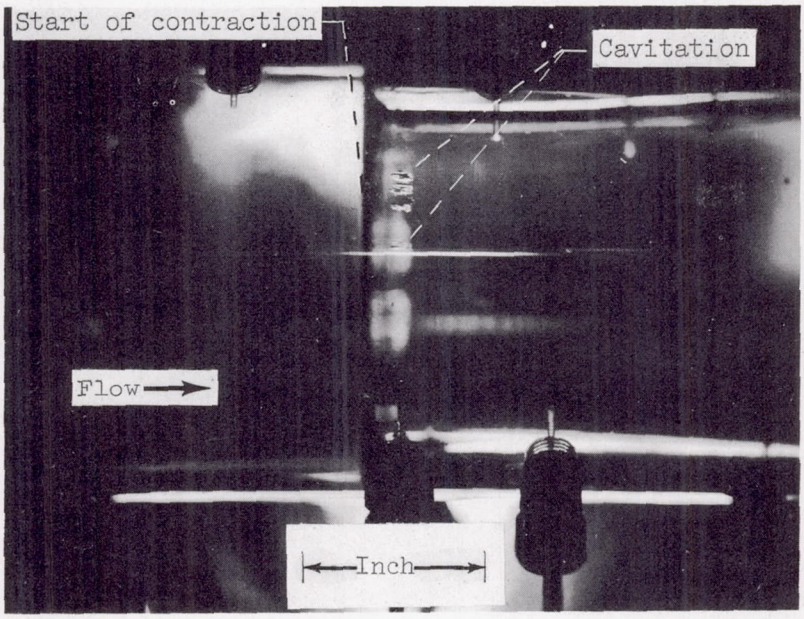

Figure 3. - Typical incipient cavitation. Free-stream velocity, 28.9 feet per second; air content, 10.0 milligrams of air per kilogram of water; temperature, 75° F; demineralized water; incipient cavitation parameter, 2.62.

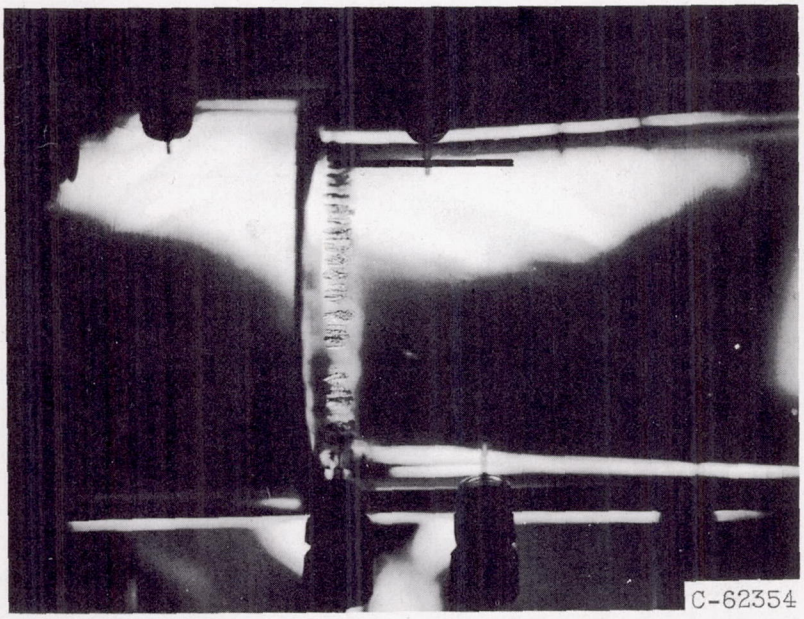

Figure 4. - Ring cavitation. Free-stream velocity, 28.8 feet per second; air content, 4.9 milligrams of air per kilogram of water; temperature, 70° F; demineralized water; cavitation parameter, 2.53.

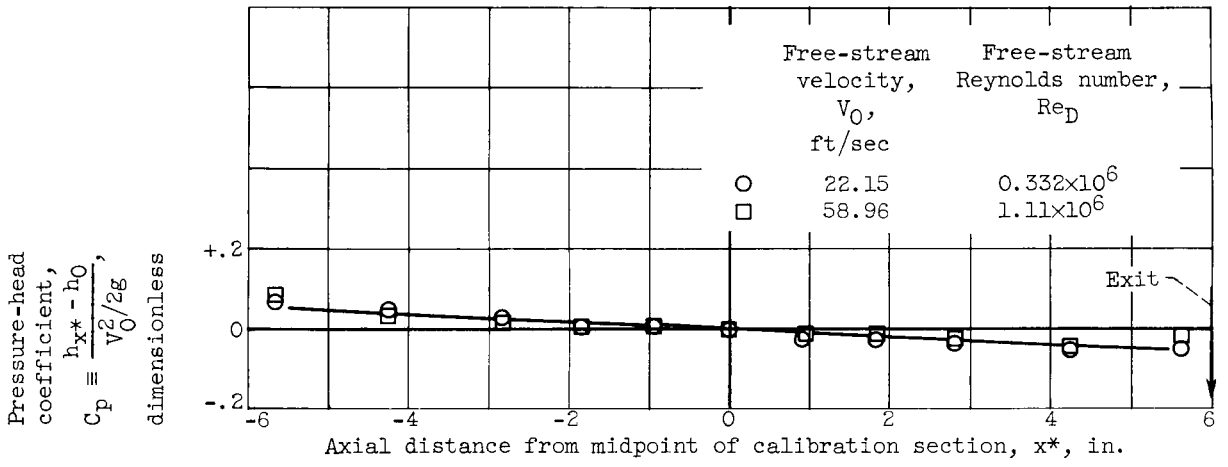

(a) Axial pressure-head distribution.

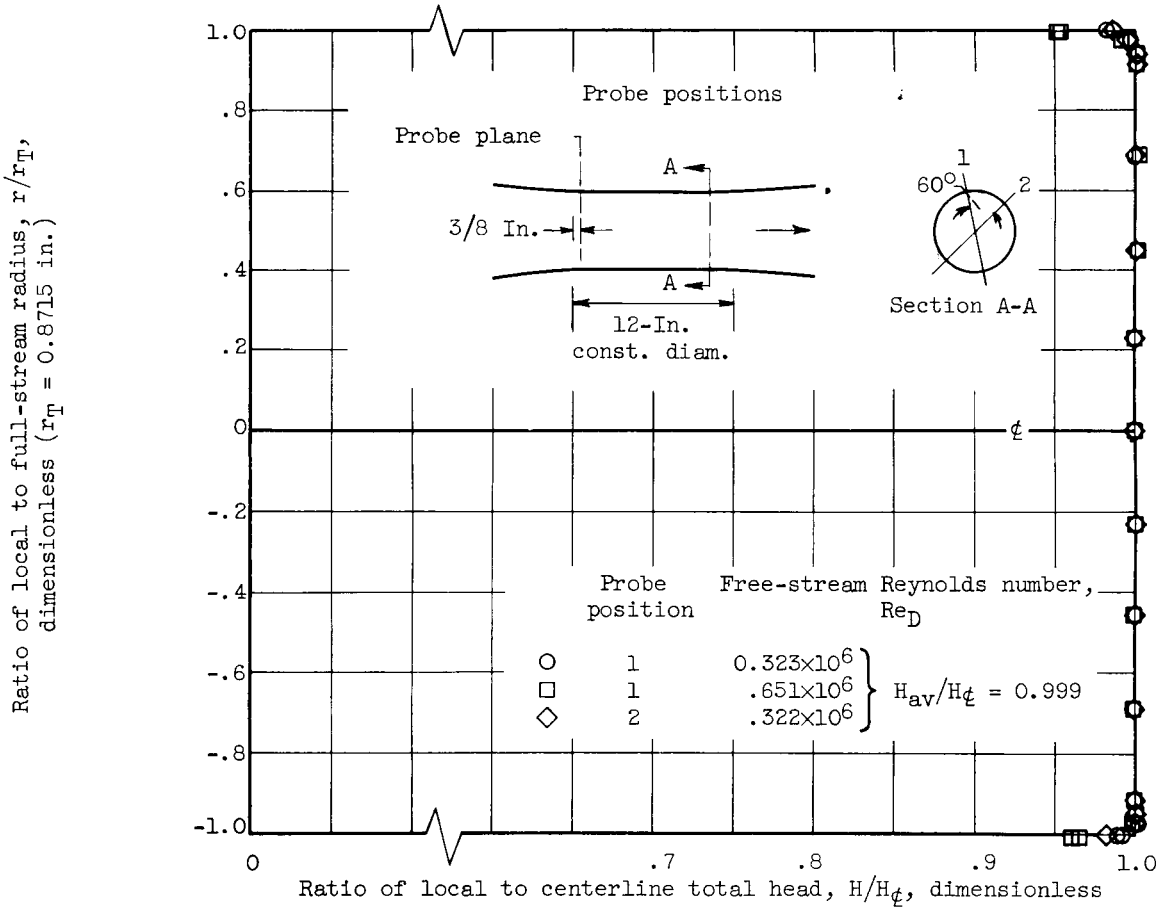

(b) Upstream total-head profile.

Figure 5. - Noncavitating performance of 1.743-inch-constant-diameter 12-inch-long calibration model.

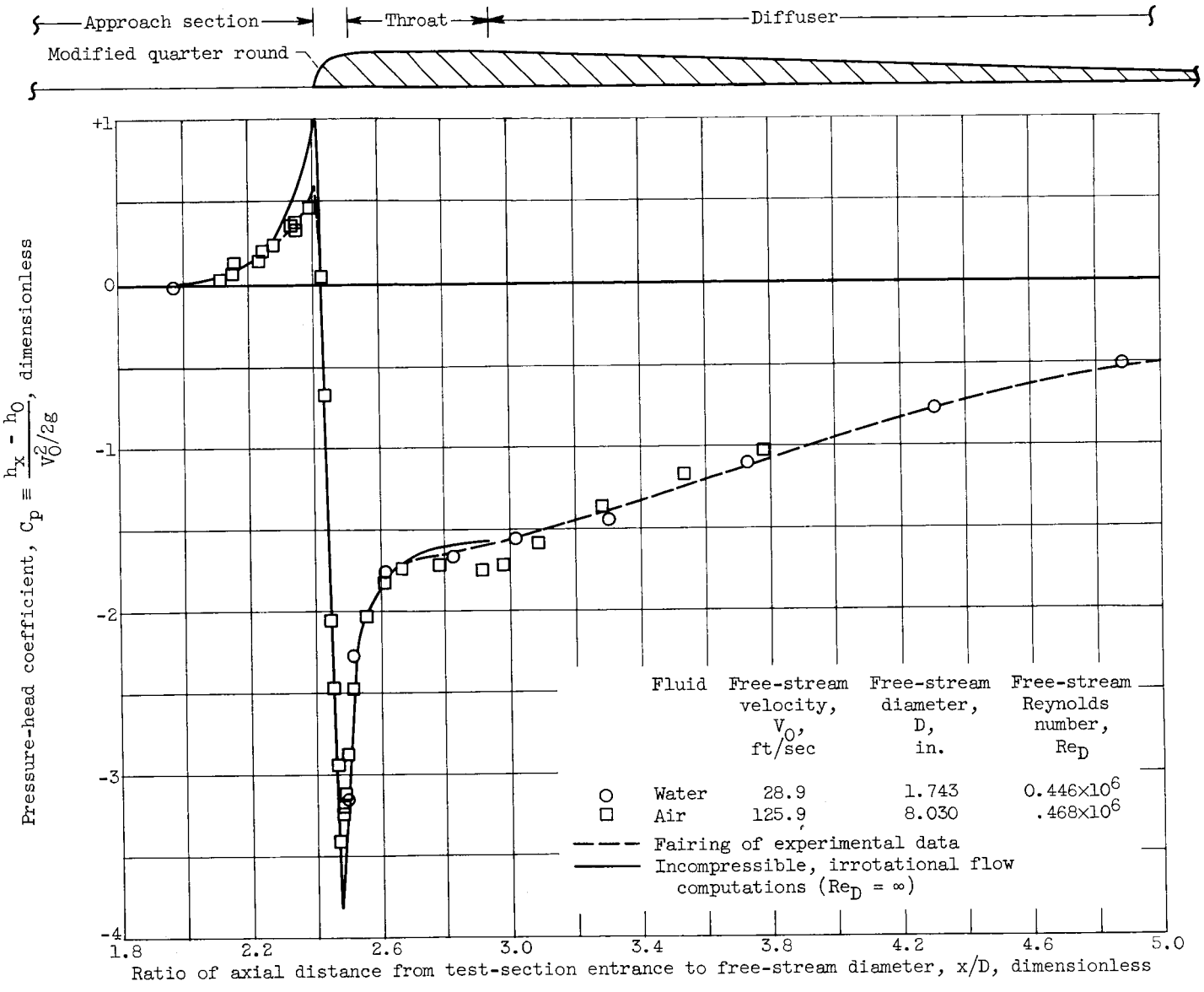

(a) Complete pressure-head distribution.

Figure 6. - Noncavitating pressure-head distribution for water- and wind-tunnel venturi models and comparison with incompressible irrotational flow computations.

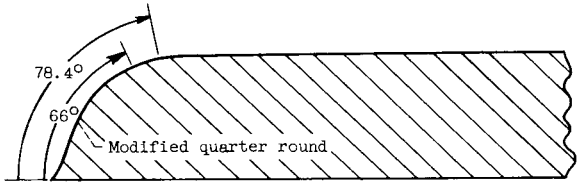

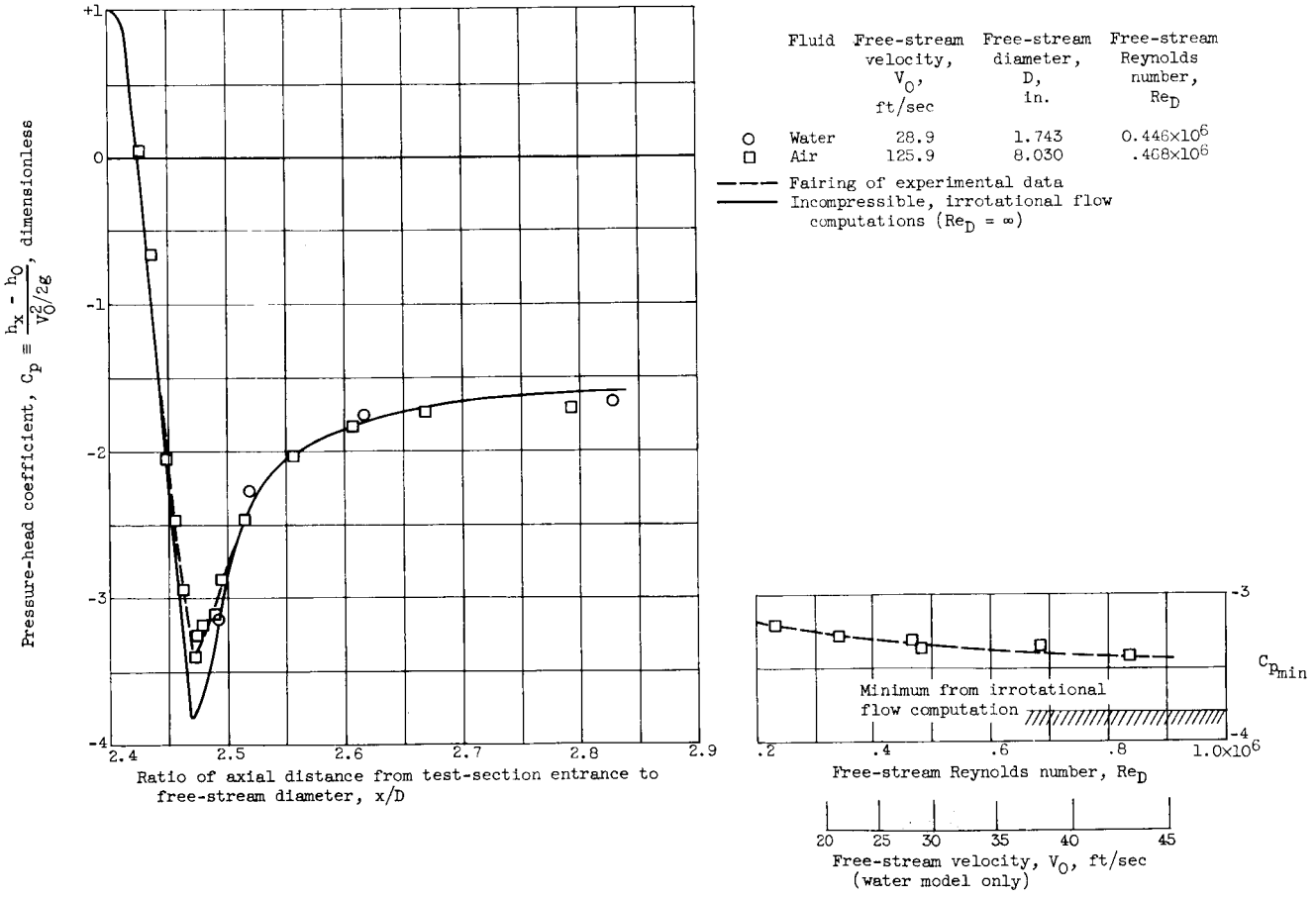

(b) Magnified plot of low-pressure region and variation of minimum pressure-head coefficient with free-stream Reynolds number.

Figure 6. - Concluded. Noncavitating pressure-head distribution for water- and wind-tunnel venturi models and comparison with incompressible irrotational flow computations.

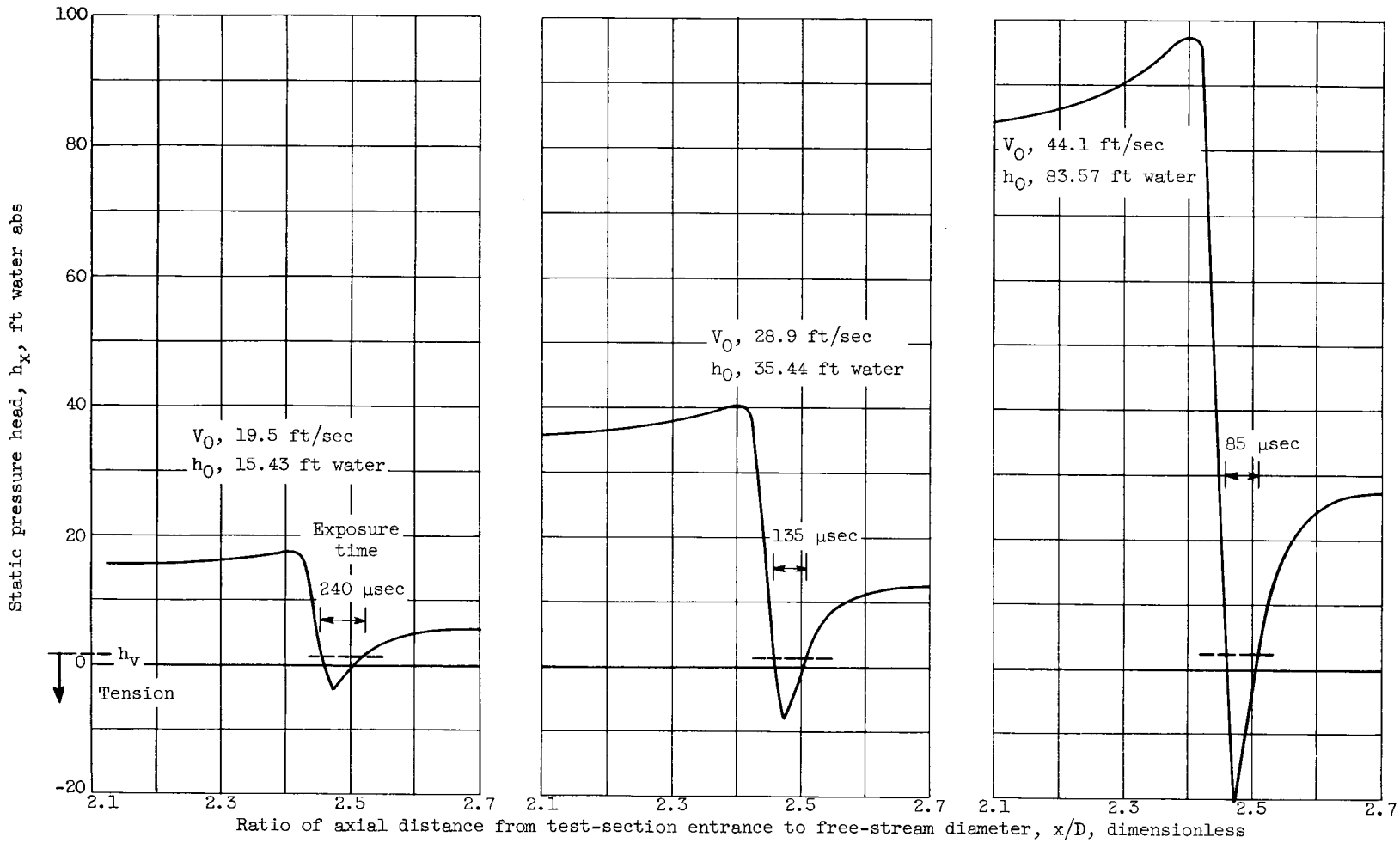

Figure 7. - Typical absolute static-pressure-head distribution at conditions of visible incipient cavitation.

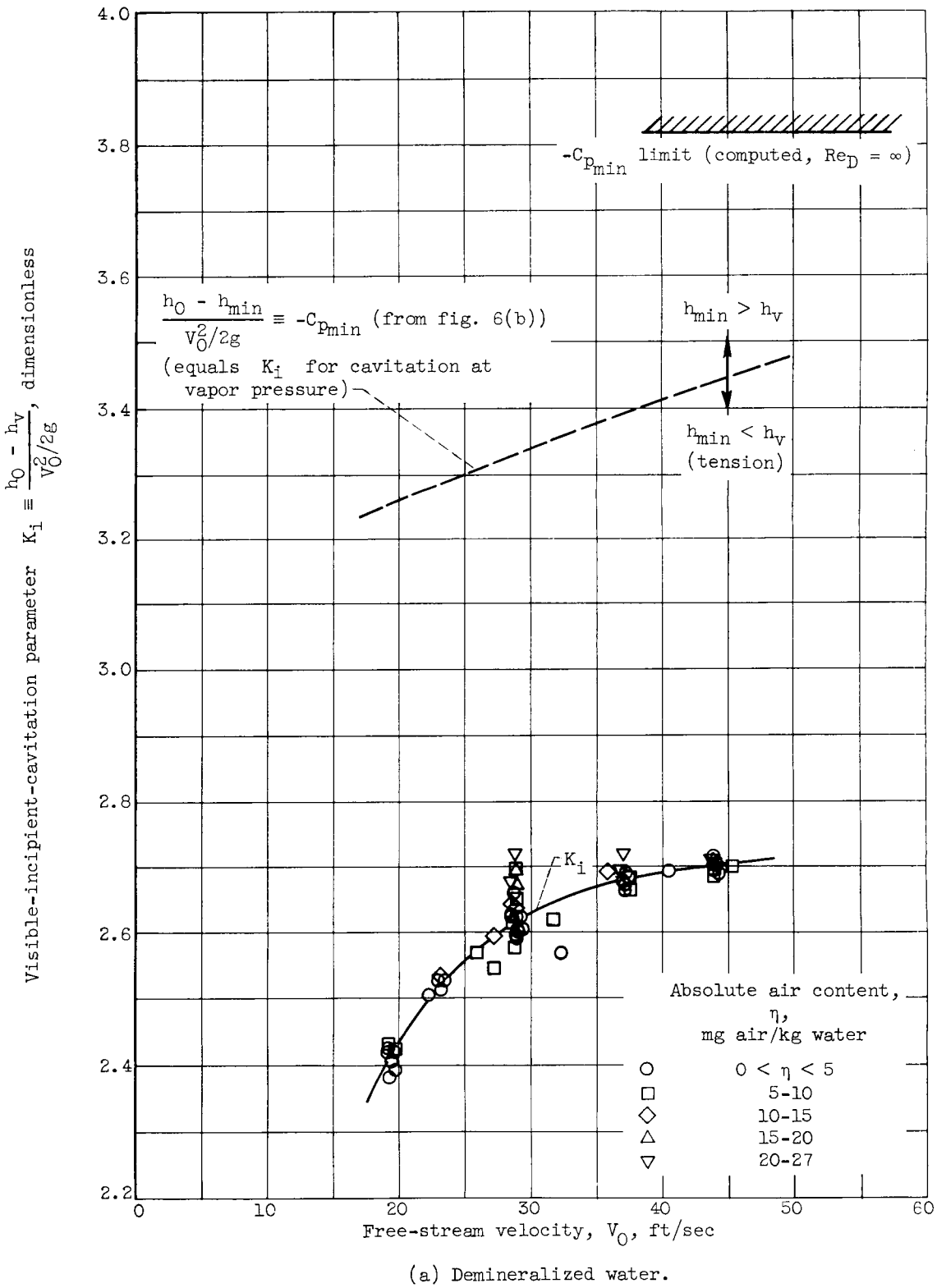

(a) Demineralized water.

Figure 8. - Visible-incipient-cavitation parameter as function of free-stream velocity and absolute air content.

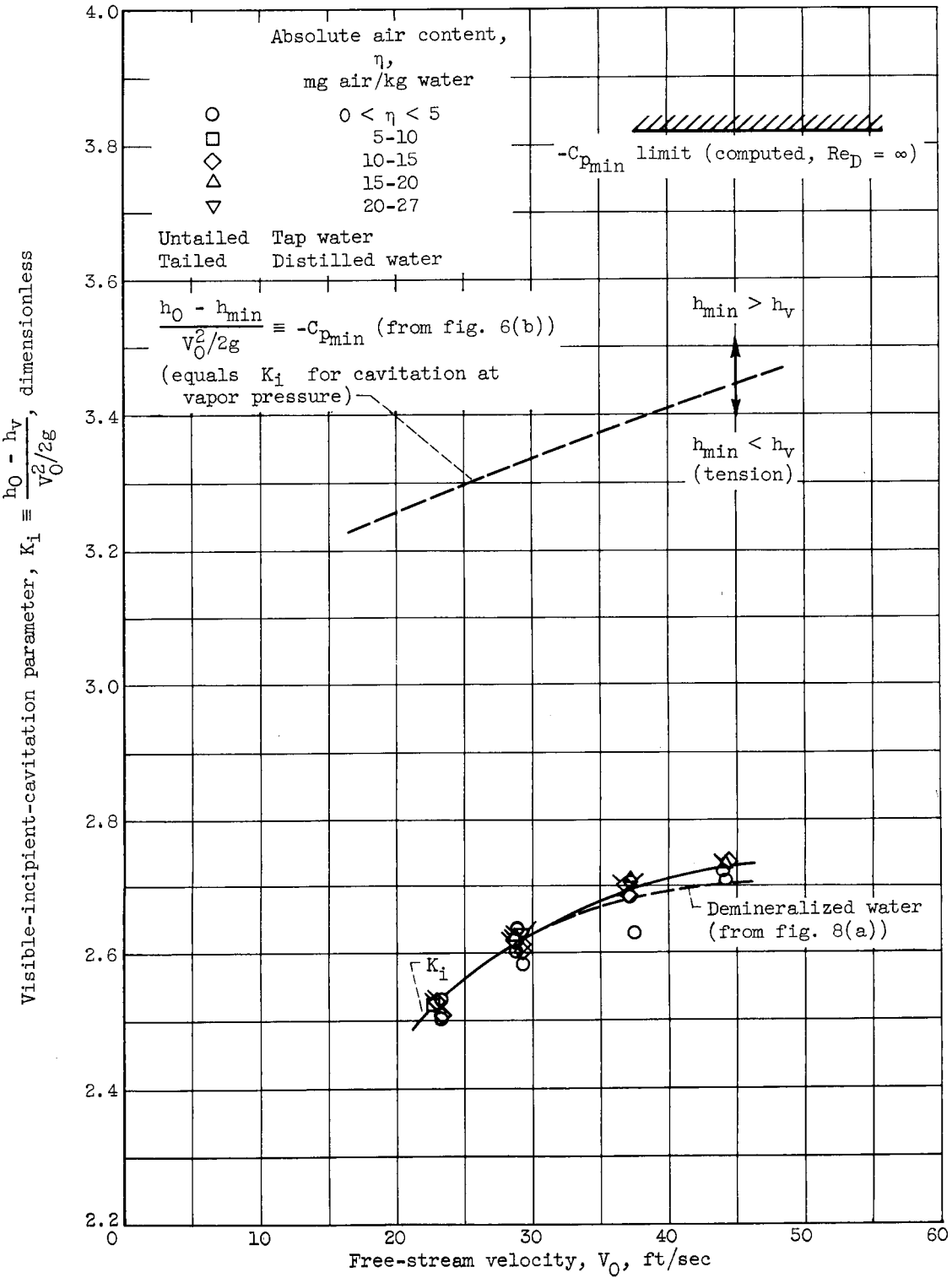

(b) Tap water and distilled water.

Figure 8. - Concluded. Visible-incipient-cavitation parameter as function of free-stream velocity and absolute air content.

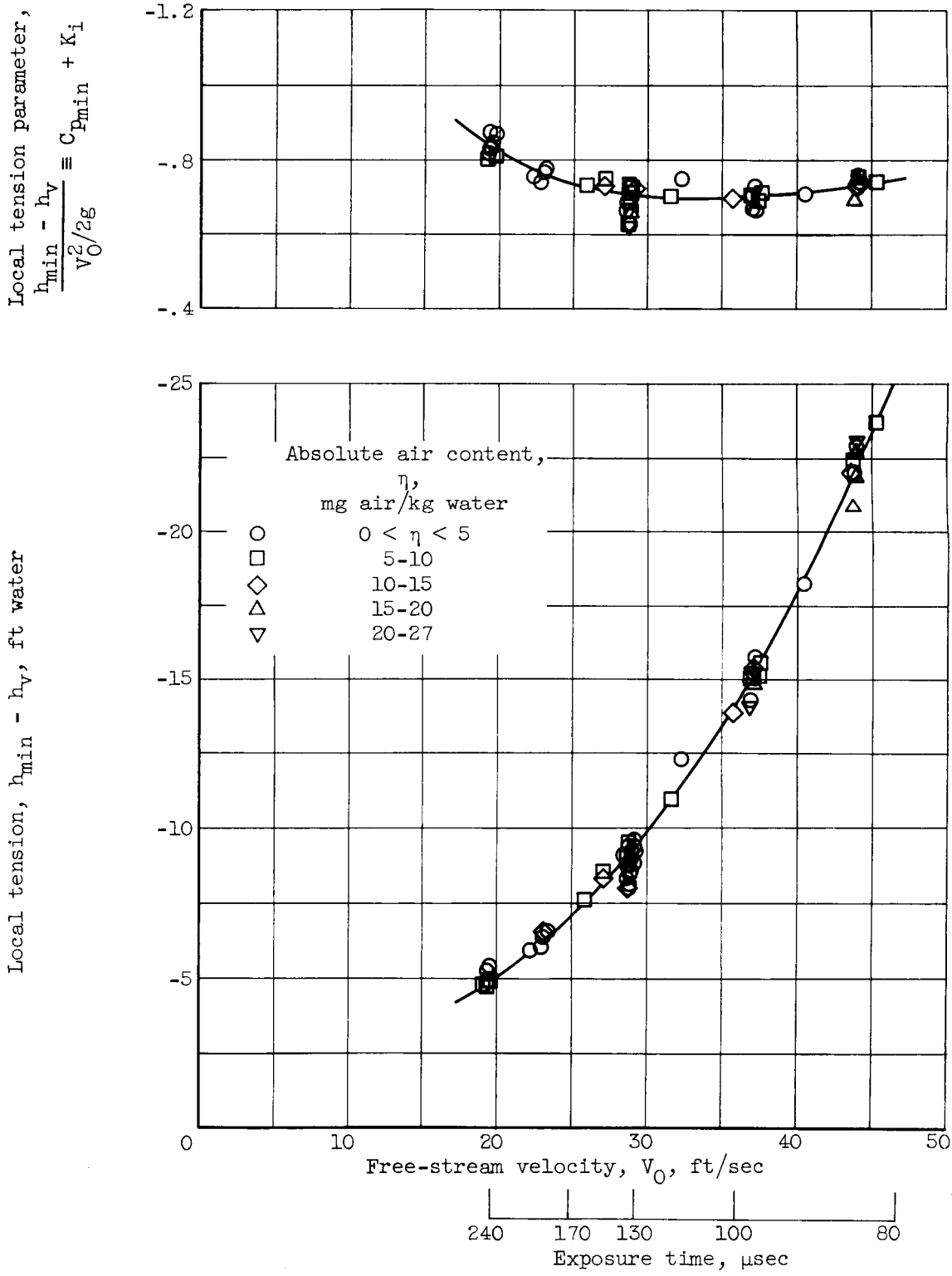

(a) Demineralized water.

Figure 9. - Local tension based on visible incipient cavitation.

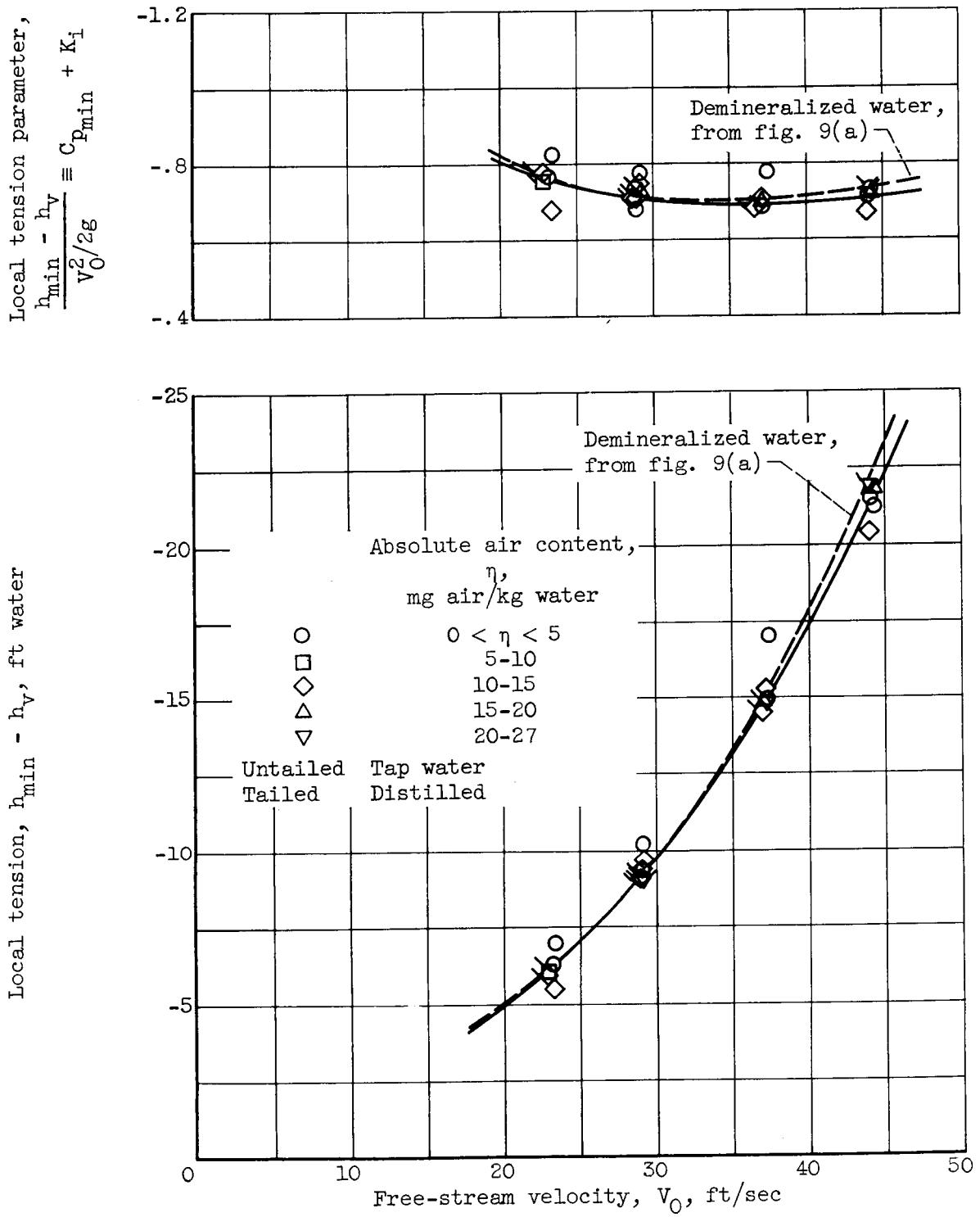

(b) Tap water and distilled water.

Figure 9. - Concluded. Local tension based on visible incipient cavitation.

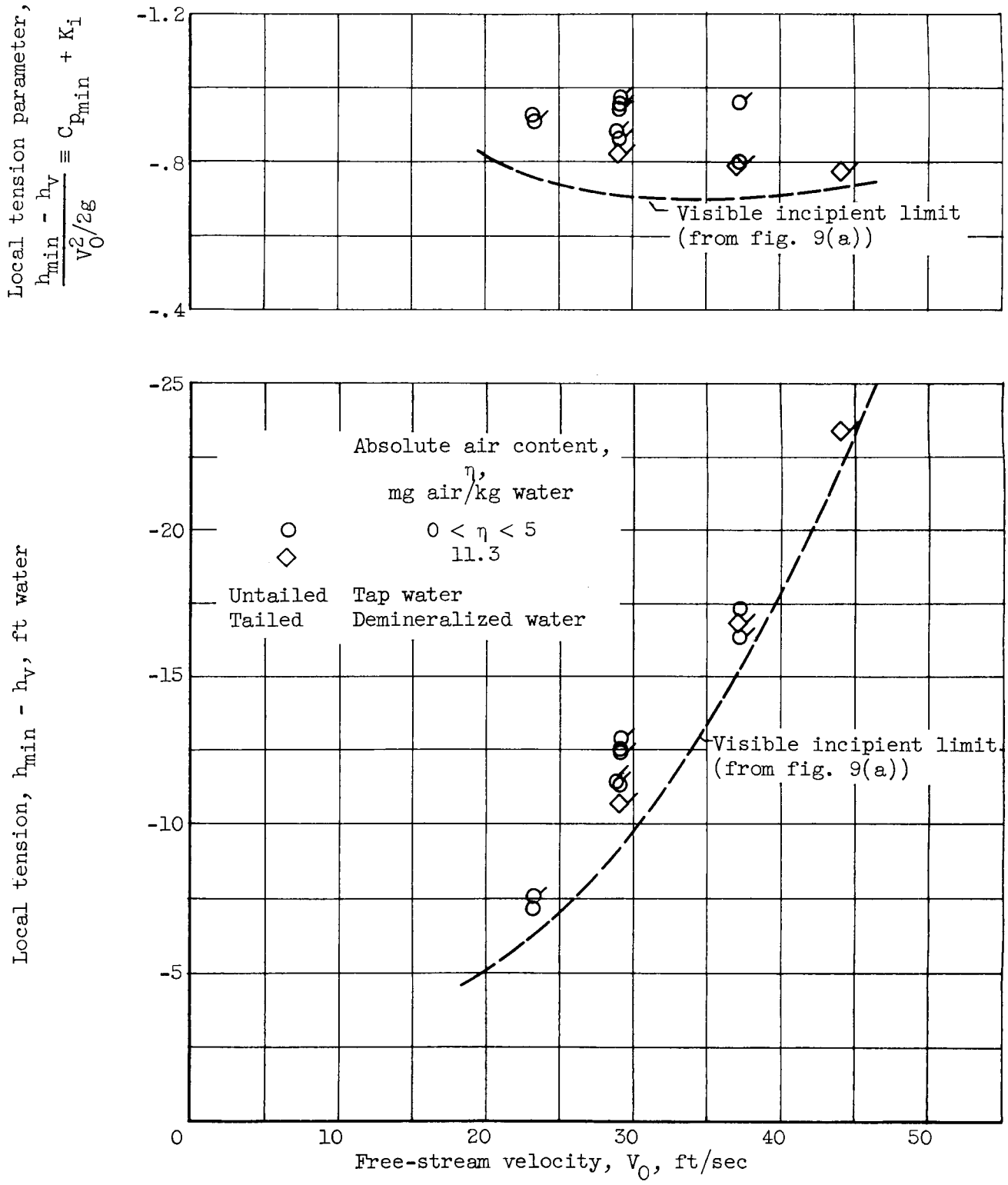

Figure 10. - Supertension (low air content only) at onset of visible cavitation.

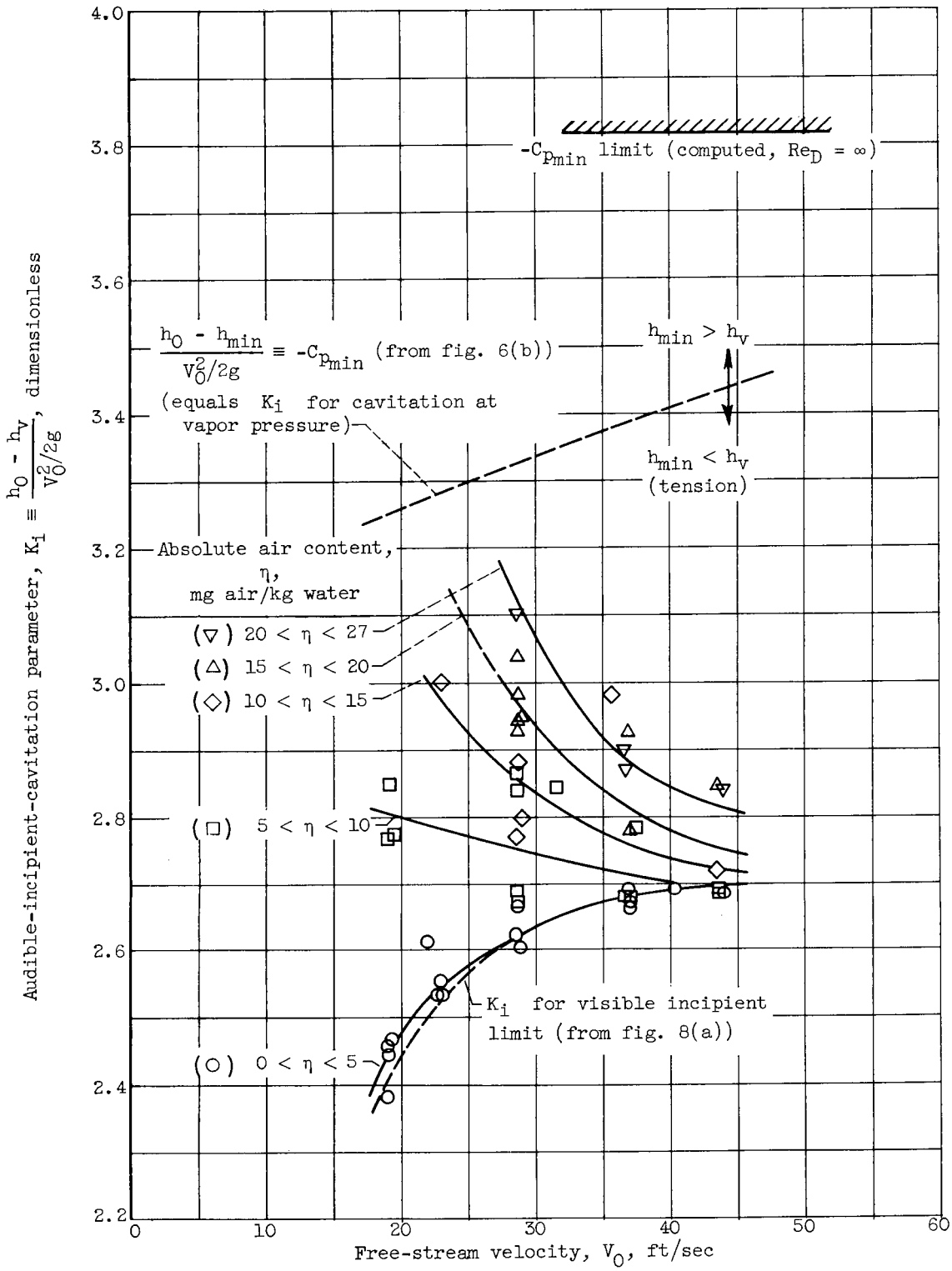

(a) Demineralized water.

Figure 11. - Audible-incipient-cavitation parameter as function of free-stream velocity and absolute air content.

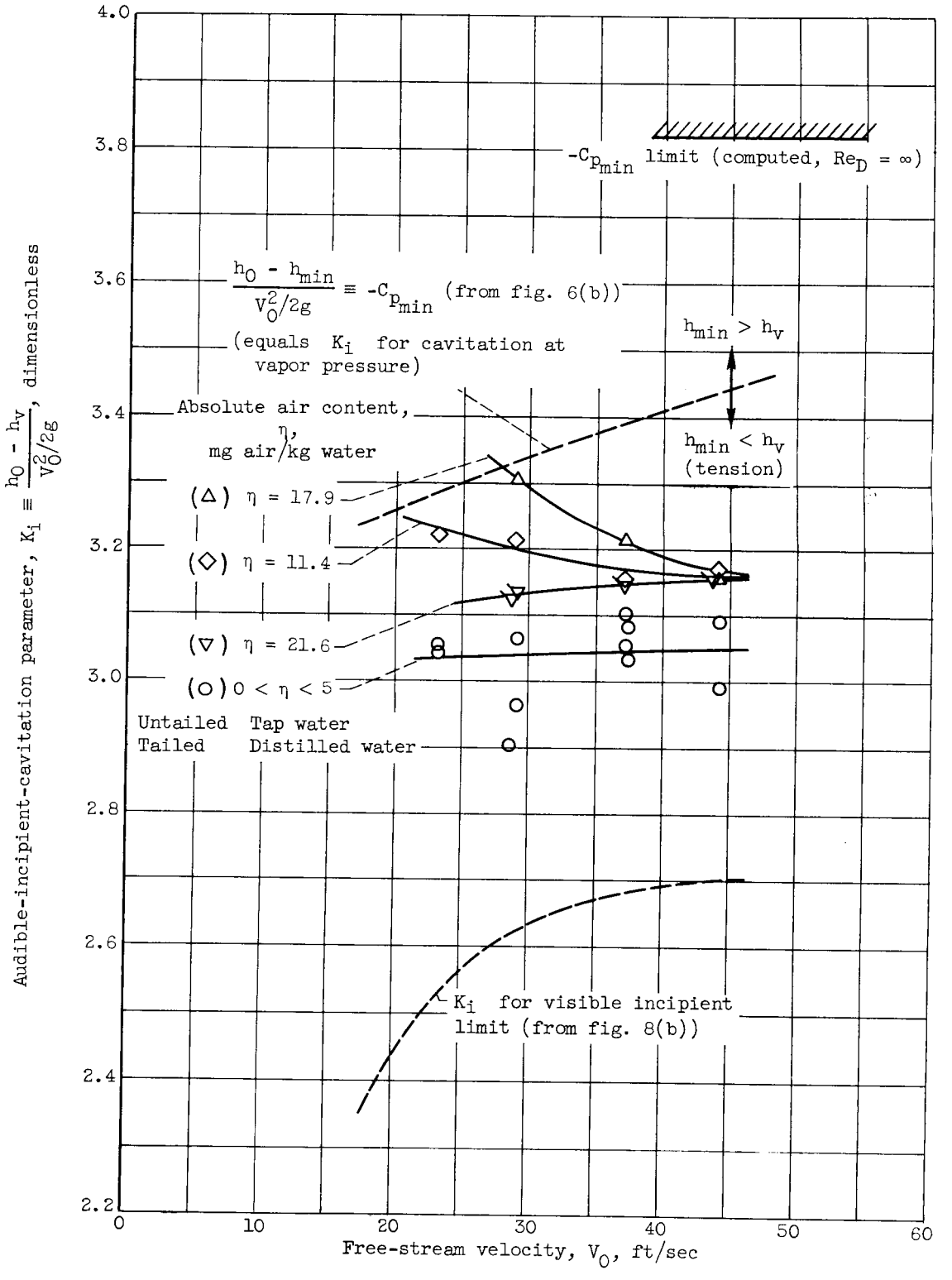

(b) Tap water and distilled water.

Figure 11. - Concluded. Audible-incipient-cavitation parameter as function of free-stream velocity and absolute air content.

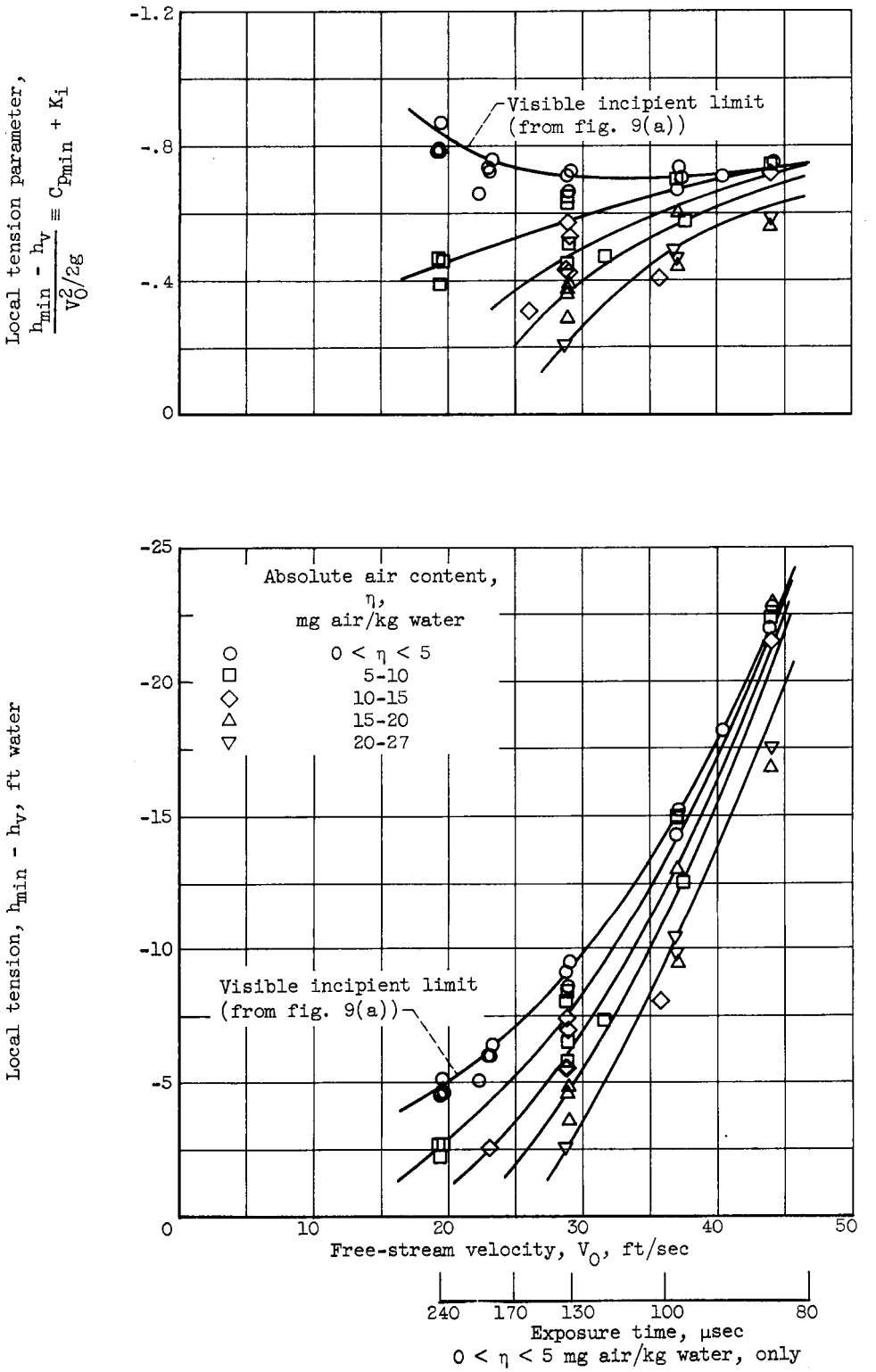

(a) Demineralized water.

Figure 12. - Local tension based on audible incipient cavitation.

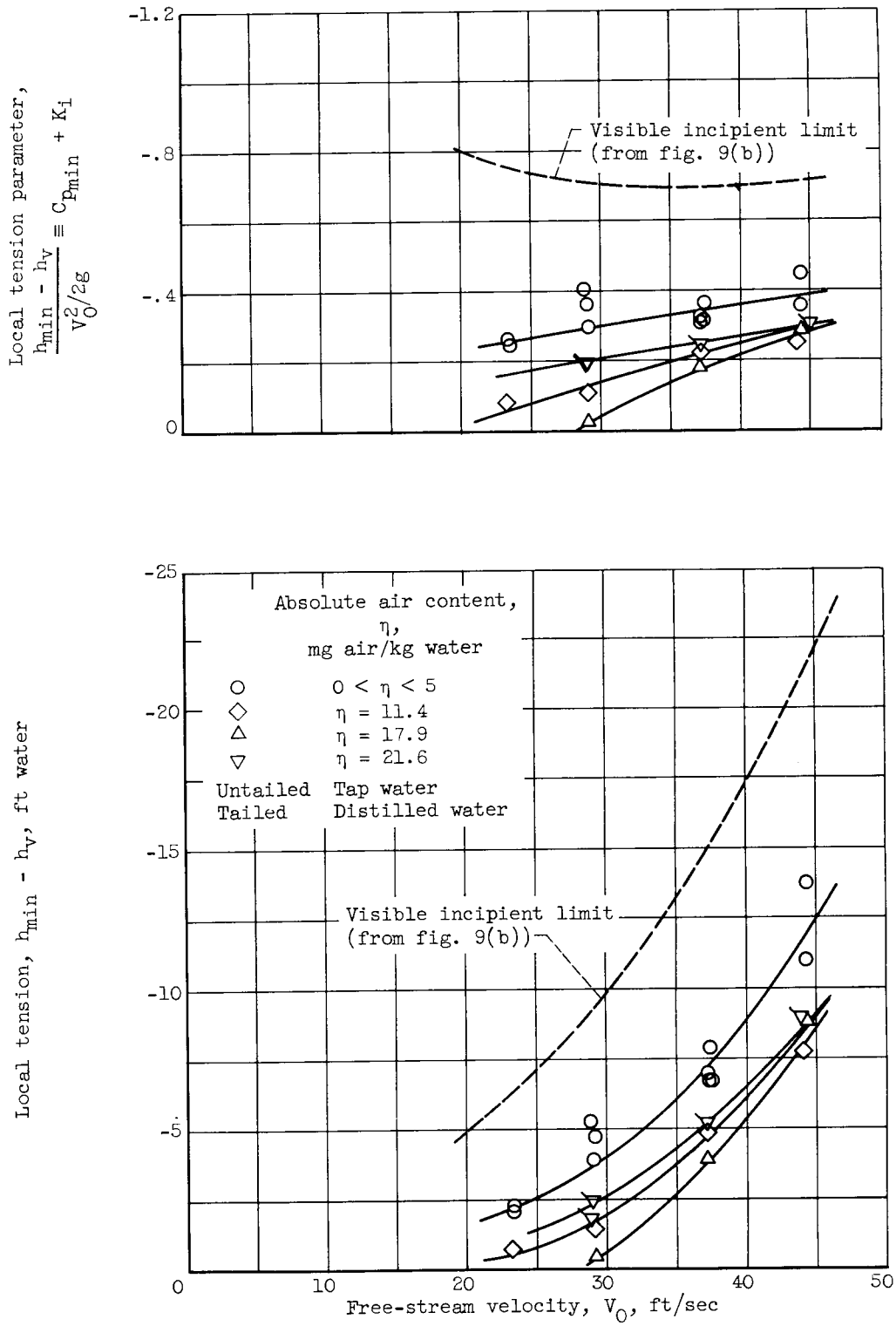

(b) Tap water and distilled water.

Figure 12. - Concluded. Local tension based on audible incipient cavitation.

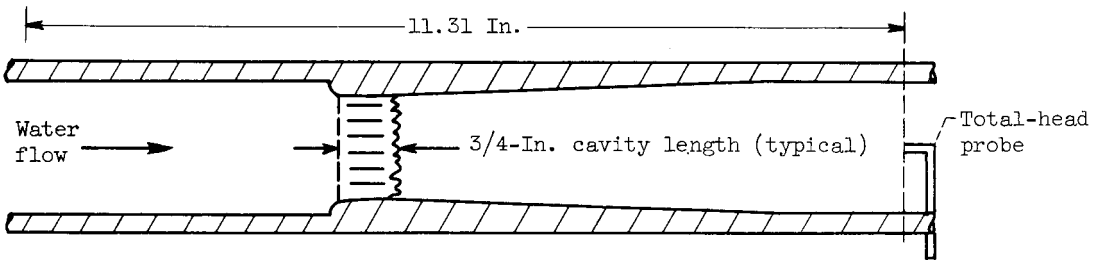

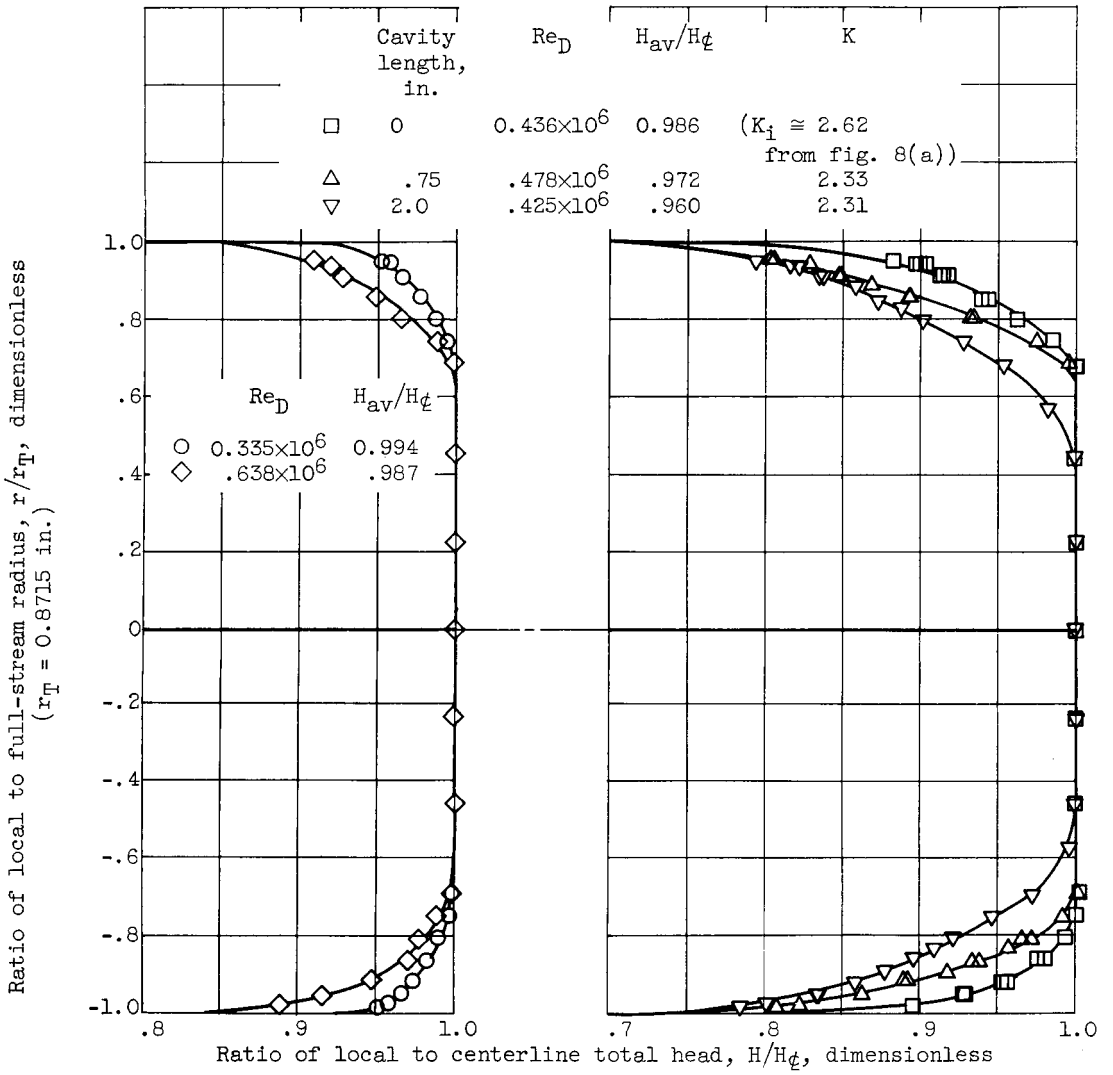

(a) Noncavitating. (b) Cavity length, 0, 3/4, and 2 inches.

Figure 13. - Downstream total-head profiles of venturi test section with various lengths of cavity. Vertical plane; axial distance from test section entrance, 11.31 inches; average free-stream velocity, 28.9 feet per second; air content, 4.7 milligrams of air per kilogram of water; average temperature, 72° F; demineralized water.

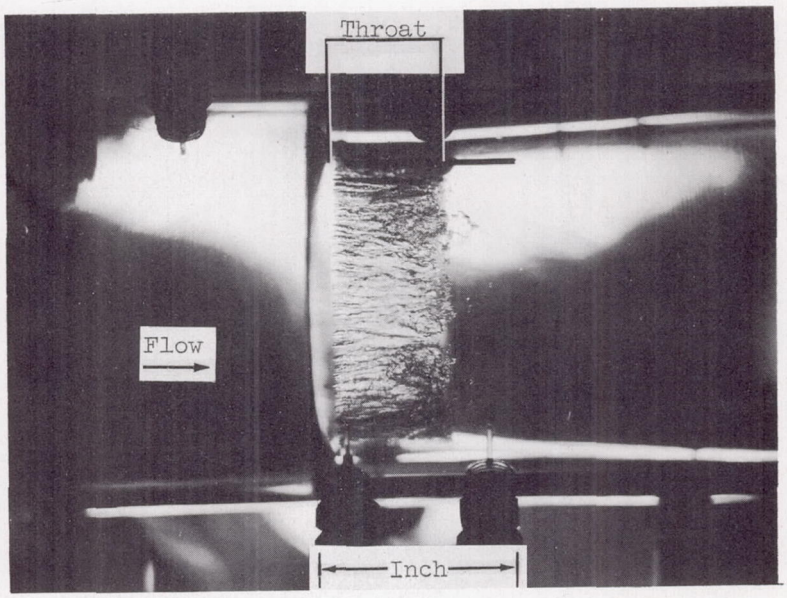

(a) 0.75-Inch-long cavitation; cavitation parameter, 2.33.

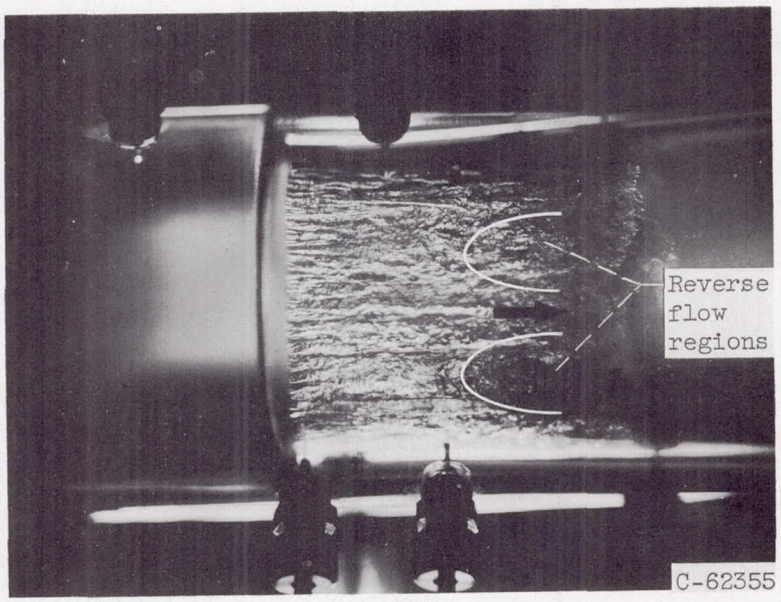

(b) 2.0-Inch-long cavitation; cavitation parameter, 2.31.

Figure 14. - Typical 0.75- and 2.0-inch cavitation associated with pressure loss data of figure 13. Free-stream velocity, 28.9 feet per second; air content, 4.7 milligrams of air per kilogram of water; average temperature, 72° F; demineralized water.

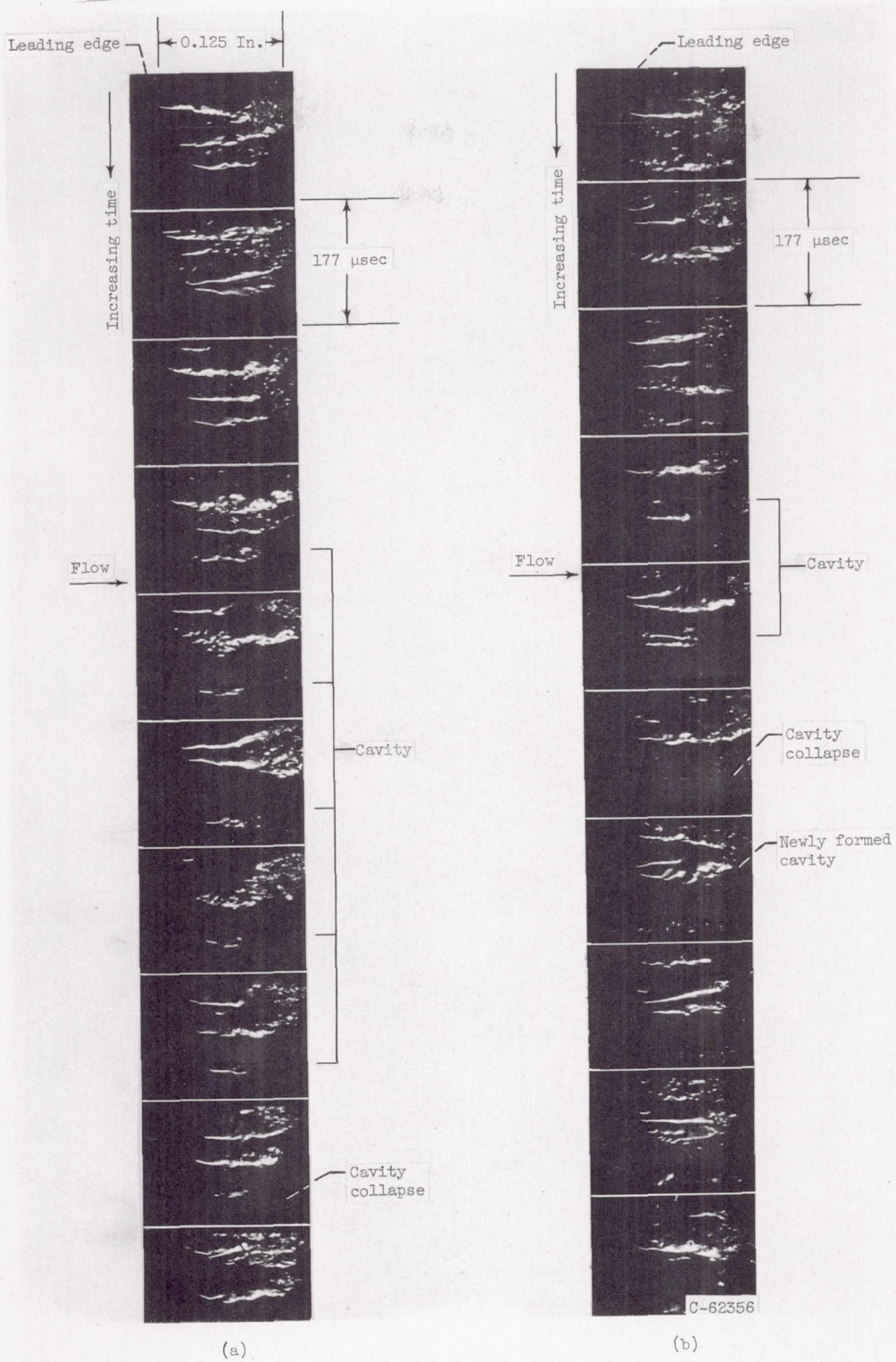

Figure 15. - Motion pictures showing leading-edge region of cavitation. Free-stream velocity, 28.6 feet per second; air content, 9.5 milligrams of air per kilogram of water; temperature, 81° F; demineralized water; cavitation parameter, 2.55; film speed, 5640 frames per second.